IEEE Access
Multidisciplinary | Rapid Review | Open Access Journal

Received August 25, 2019, accepted September 23, 2019, date of publication September 27, 2019, date of current version October 16, 2019.

Digital Object Identifier 10.1109/ACCESS.2019.2944217

Influence Analysis of the Elastic Supporting to the Dynamic Response When the Spherical Rock Elastic Impacting the Metal Plate and to the Coal Gangue Impact Differences

YANG YANG[1], (Student Member, IEEE), AND QINGLIANG ZENG[1,2]
[1]Department of Mechanical and Electrical Engineering, Shandong University of Science and Technology, Qingdao 266590, China
[2]College of Information Science and Engineering, Shandong Normal University, Jinan 250358, China

Corresponding author: Qingliang Zeng (qlzeng@sdust.edu.cn)

This work was supported in part by the National Natural Science Fund of China under Grant 51674155 and the National Natural Science Fund of China under Grant 51974170, in part by the Innovative Team Development Project of Ministry of Education under Grant IRT_16R45, in part by the Special Funds for Climbing Project of Taishan Scholars, and in part by the Postgraduate Science and Technology Innovation Project of the Shandong University of Science and Technology under Grant SDKDYC190108.

ABSTRACT This paper takes the impact and collision behavior between coal gangue granule and the hydraulic support during the top coal caving mining as the research subject. The impact-contact dynamic model when the rock sphere impact on the any axial direction position of the bilateral fixed supporting, bilateral elastic supporting, and unilateral elastic unilateral fixed supporting metal plate is established respectively, which is conducted with the full consideration of the Flores contact theory (contain the elastic force and damping force), the bending deformation and energy absorption theory of the simply supported beam and the cantilever beam, and the constant stiffness spring compression deformation and energy absorption theory. And the maximum contact responses such as the max contact force, the max sphere rock compression, the max deflection of the metal plate and the max system energy conversion ratio are solved on the basis of the energy conservation law and the recursive solution method. After that, the rock yield velocity when the rock sphere impact on the different supported metal plates is obtained. Finally, we analyze the effects of the elastic supporting, the impact position and the spring stiffness on the yield velocity. The influence of the elastic support, the impact position, the spring stiffness and the metal plate length on the system contact response, as well as the influence of the elastic support on the coal gangue impact response differences are analyzed within the elastic impact velocity range. The research conclusions will provide theoretical references for the contact response problems when the sphere vertical impact on any position of the flexible plate and impact the elastic supporting structures, and provides research foundation for the study of impact behavior in the top coal caving mining between the coal gangue granule and the hydraulic support.

INDEX TERMS Coal gangue, impact, elastic supporting, spring stiffness, contact, response difference.

I. INTRODUCTION

The mining of top-coal caving [1]–[4] refers to that a mining face with a height of 2∼3m along the bottom plate of a coal seam or the bottom of a certain thickness within the seam will be arranged when mining the thick coal seams. And then the fully-mechanized mining will be utilized in the process of recovery. By means of the mine pressure or assisted by the method of loosening blasting, the top coal will be broken into the loose body and it is released from the "window" behind or above the support, and then it is transported out of the working face by scraper conveyor.

In the releasing process of top-coal caving, the hydraulic powered support for the mining of top-coal caving [5], [6] (as shown in Figure 1) plays an important role in many aspects, including in the basic control items, the function of maintaining immediate roof, self-moving and pushing conveyors, and controls of the mechanism in the process of top-coal releasing, falling-coal blasting and large-coal blasting, as well as float-coal cleaning. In this process, the top beam, tail beam

The associate editor coordinating the review of this manuscript and approving it for publication was Zhixiong Peter Li.

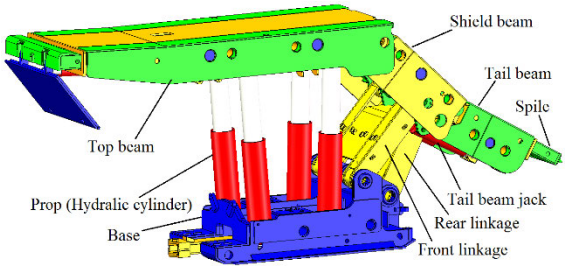

FIGURE 1. Hydraulic powered support for the mining of top-coal caving.

and caving shield (especially the tail beam) must be vertically or tendentiously impacted by the coal gangue particles, or the coal gangue particles will slip along various parts of the overlying strata metal plate. Impact-contact behavior between coal gangue particles and the metal plate can be considered as the typical mechanics behavior in the top coal caving process.

As a typical contact mechanics, impact-contact behavior between spheres [7]–[16] and between sphere and plane body or space body [17]–[30] have been further studied by many scholars at home and abroad. Solely based on material properties and contact geometries, Brake [31] put forward a new computational formulation for the normal direction's elastic-perfectly plastic contact between two round surfaces. Through the experiment and the finite element simulation using LS-DYNA software, Minamoto and Kawamura [32] researches the influence of the strain rate sensitivity on the impact of two identical spheres. Jamari and Schipper [33] presents an elastic–plastic contact model for the ellipsoid bodies, the functional relation between the contact parameters and the contact interference are modeled in different contact regimes, and the model is verified by the experimental results and compared with the published theoretical models. To ensure the accuracy and efficiency of the granular-flow simulation, Vu-Quoc *et al.* [34] put forward an elasto-plastic frictional tangential force–displacement model for the contacted spheres. Jackson *et al.* [35] research the recovery coefficient of the impacting elastic-perfectly plastic spheres and establishes the formula of the initial critical speed which causes the initial plastic deformation of the sphere. Vu-Quoc *et al.* [36] presents an elastoplastic NFD model for the impacted spheres, and the simulation of the sphere impacting with the frictionless rigid planar surface is conducted. By the combination of the traditional contact model and the influence coefficients, Wang *et al.* [37] propose the point contact model between the rigid ball and the elastic coated solid. Thornton *et al.* [38] studied the various elastic plastic normal contact force models through the normal impact between the sphere and the target wall. Peng *et al.* [39] obtain the contact responses such as the contact force, the relative penetration and the velocity of the sphere-plane contact by finite element simulation method and then estimated the contact stiffness, the hysteresis damping factors, and the elastic impact index through a theoretical model. Yang *et al.* [40] studied the contact response when the elastic sphere impact on the elastic half space through the FEM simulation. In order to theoretically solve the unknown parameters such as the instantaneous velocity and instantaneous compression deformation of the elastic sphere during impact-contact process, Bischoff et al. proposed a simple spring-mass model to describe the relation between the contact force and the time under the condition of ignoring the system damping energy [41]. According to the forces of nonlinear spring and linear damping, Rigaud *et al.* [42] established a system nonlinear dynamic equation on the basis of the single degree-of-freedom oscillator. The researches above have provided theoretical references, simulation and experimental methods for the study of impact-contact behavior between spheres, between sphere and plane/flat/elastic half space. However, they have failed to involve the impact behavior between rock and metal plate, and the elastoplastic deformation of the rock mass's impact. Moreover, the self-bending deformation and energy absorption of thin plates such as the metal plate have not been taken into consideration during the impact-contact behavior. And Yang *et al.* [43] studied the initial yield velocity of the sphere when the rock impacts the center of the metal plate which is fixed, but did not study the response when the rock impacting the metal plate under multi-support conditions such as the flexible supported metal plate, as well as the contact model of the system when the rock impact on any axial direction position of the metal plate.

During the whole releasing process of top coal caving, vertical or oblique impacts between the coal gangue particles and the overlying strata metal plate of the top beam, caving shield and tail beam will occur. As is shown in Figure 2, according to the structure of the hydraulic powered support for the top coal caving mining, the top beam is directly supported by props (drive device) on both ends and shield beam (The follow-up device) which is fixed by the top beam and the front and rear linkages. In addition, the tail beam is supported by the shield beam and the tail beam jack. The prop and the tail beam jack are the flexible energy-storage device. Therefore, three different collision contacts in the top coal caving process are exist, which is the contact when coal gangue impacting the fixed supported metal plate, the contact when coal gangue impacting the bilateral prop supported metal plate, and the contact when coal gangue impacting the unilateral fixed unilateral tail beam jack supported metal plate respectively. Moreover, because of the complex working environment and the large number of particles, the metal plate may be impacted by particles at any position.

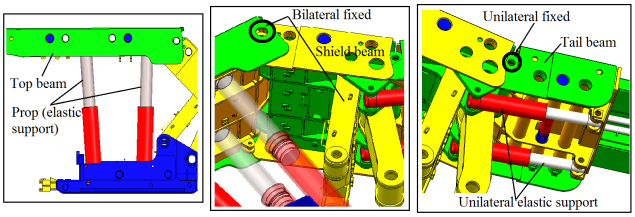

FIGURE 2. Supporting states of the hydraulic powered support.

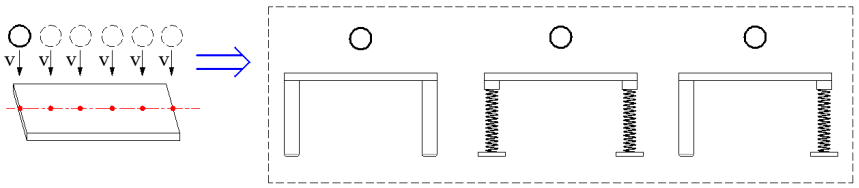

FIGURE 3. Equivalent conditions.

In order to qualitatively investigate the contact response of the particle body and the metal plate induced by the impact between particles and the hydraulic support during the top coal caving, the complex supporting structures of the top beam, the shield beam and the tail beam are simplified into the bilateral fixed supporting metal plate structure (Define as working condition 1 or Con 1), the bilateral elastic supporting metal plate structure (Define as working condition 2 or Con 2), and the unilateral elastic unilateral fixed supporting metal plate structure (Define as working condition 3 or Con 3) respectively, as is shown in Figure 3. This paper takes the multiform supporting metal plate which any axial position is impacted by the single spherical coal gangue particle as the research object. On the basis of the Flores contact model and combine with the bending deformation and energy absorption theory of the simply supported beam and cantilever beam, as well as with the consideration of the energy consumption in the rock sphere compression process, the energy absorbed by the elastic supporting device and by the metal plate, the impact-contact model when the rock sphere impact on the any axial direction position of the bilateral fixed supporting metal plate, bilateral elastic supporting metal plate, and unilateral elastic unilateral fixed supporting metal plate is established respectively. According to the recursive solution method, the maximum contact responses at the critical end of the compression process such as the contact force, the spherical rock compression, the deflection of the metal plate and the system energy conversion ratio are solved. Through the Drucker-Prager criterion, the rock yield velocity model when the spherical rock impacting the any axial direction position of the bilateral fixed supporting, bilateral elastic supporting, and unilateral elastic unilateral fixed supporting metal plate is obtained. Combine with the approximate theoretical solution of these maximum contact response and the yield velocity model of the rock sphere, the effects of the elastic support, impact position, spring stiffness and the length of metal plate to the yield velocity, the system contact response and the coal gangue impact response differences are discussed and studied.

The paper is organized as follows. Introduction is presented in Section 1. Section 2 establishes the system contact model when the rock sphere impacting the any axial direction position of the bilateral fixed supporting metal plate, the bilateral elastic supporting metal plate, and the unilateral elastic unilateral fixed supporting metal plate. Section 3 deduces the rock yield velocity model when the spherical rock impacting the three different supporting form metal plates. Section 4 analysis the effects of the elastic support, impact position, spring stiffness and length of metal plate to the yield velocity and the system contact response, and discusses coal gangue impact response differences and the effects of the elastic support to the coal gangue impact response differences. Finally, some related work and concluding remarks are given in Section 5.

II. SYSTEM DYNAMIC MODEL WHEN THE SPHERICAL ROCK ELASTIC IMPACTING THE ANY AXIAL POSITION OF THE DIFFERENT SUPPORTING FORM METAL PLATE

According to the Hertz contact theory in statics [44]–[49], Flores [50], Flores *et al.* [51]–[53], and Alves *et al.* [54] put forward a system contact model with the consideration of the damping force and the loss in energy triggered by the system damping:

$$P = K\delta^n + D\dot{\delta} \tag{1}$$

$$\dot{\delta} = \delta^{(\cdot)}\sqrt{1 - (\frac{\delta}{\delta_{\max}})^2} \tag{2}$$

$$K = \frac{4\sqrt{R}}{3} \cdot E \tag{3}$$

$$\frac{1}{E} = \frac{1-\mu_1^2}{E_1} + \frac{1-\mu_2^2}{E_2} \tag{4}$$

$$\frac{1}{R} = \frac{1}{R_1} + \frac{1}{R_2} \tag{5}$$

where P is the Flores contact force, E_1, μ_1, E_2, μ_2 represent the elastic modulus and Poisson's ratio of the elastic sphere and the impacted sphere or the plate respectively, K is the contact stiffness, E is the equivalent elastic modulus, n is the nonlinear exponent and $n = 3/2$, R_1 and R_2 is the contact radius of the two contact medium, (The contact radius of the plate goes to infinity, in this paper, R_2 goes to infinity, so the equivalent contact radius $R = R_1$), δ is the compression deformation, $\delta_{\max}$ is the maximum compression deformation, the damping coefficient $D = K\delta^n \cdot \frac{8(1-e)}{5e\dot{\delta}^{(-)}}$, $\dot{\delta}^{(-)}$ is the initial relative velocity (i.e. the initial velocity v_1 of the sphere in this paper), $\dot{\delta}$ is the instantaneous velocity, e is the restitution coefficient.

The energy absorbed and consumed by the rock sphere W_Q in the process of compression deformation under the contact force is as follows:

$$\begin{aligned} W_Q &= \int_0^{\delta} P d\delta \\ &= \frac{2}{5}K\delta^{\frac{5}{2}} + \frac{8K(1-e)}{5e}\int_0^{\delta} K\delta^n \cdot \frac{8(1-e)}{5e\dot{\delta}^{(-)}} d\delta \end{aligned} \tag{6}$$

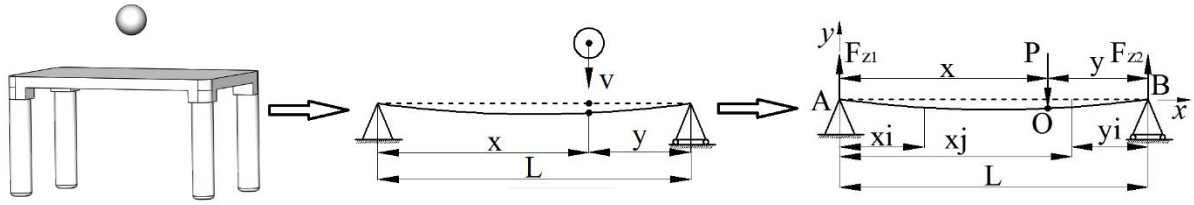

FIGURE 4. Bending deformation in the axial direction of the metal plate under bilateral fixed supporting.

Combining Eq. (2) and literature [55], the total energy absorbed and consumed by the rock sphere at the critical end of compression is obtained as follows:

$$W_{QZ} = \frac{2}{5}K\delta_{\max}^{\frac{5}{2}} + \frac{8K(1-e)}{5e}\int_0^{\delta_{\max}} \delta^{\frac{3}{2}}\sqrt{1-\left(\frac{\delta}{\delta_{\max}}\right)^2}\,d\delta = \frac{2K}{5e}\delta_{\max}^{\frac{5}{2}} \tag{7}$$

A. DYNAMIC MODEL WHEN THE ROCK SPHERE IMPACTING THE BILATERAL FIXED SUPPORTING METAL PLATE

From Figure 4, under the action of the concentrated force of P, the support forces at the ends of the beam are obtained as follows:

$$F_{z1} = \frac{Py}{L}, \quad F_{z2} = \frac{Px}{L}, \quad x + y = L \tag{8}$$

where L is the length of the metal plate, x is the distance from the left end A of the metal plate to the impact point O which the sphere rock impact on the metal plate, y is the distance from the right end B of the metal plate to the impact point O.

The deflection-curve equation of simply-supported beam is obtained as follows:

$$\begin{cases} E_L I\omega_{xi} = -\dfrac{Py}{6L}\cdot xi\cdot\left(L^2 - y^2 - xi^2\right) \\ E_L I\omega_{yi} = -\dfrac{Py}{6L}\cdot\left[(L^2 - y^2 - xj^2)\cdot xj + \dfrac{L}{y}(xj - x)^3\right] \end{cases} \tag{9}$$

In Eq. (9), E_L is the elastic modulus of the beam, I is the moment of inertia of the beam, xi is the point which it's distance from the left end of the beam (metal plate) is xi (the point is between the A and O), yi is the point which it's distance from the right end of the beam (metal plate) is yi (the point is between the B and O), and xj = L − yi, ω_{xi} and ω_{yi} is the deflection of the point xi and yi.

At this time, the deflection (value) at point O of the concentrated force P is as follows:

$$\omega_O = \frac{Py}{6E_L IL}\cdot x\cdot\left(L^2 - x^2 - y^2\right) \tag{10}$$

As for the condition where the four corners of the metal plate are subjected to the fixed support (Figure 4), in order to simplify the calculation, only the axial bending deformation is considered and it can be equivalent to the simply-supported beam. Define $I_2 = \frac{Bh^3}{12}$ (where E_2, I_2, B and h is the elastic modulus, moment of inertia, the width and the thickness of the metal plate respectively), when the rock sphere impacts on any axial direction position of the metal plate, according to the Eq. (1) and Eq. (10), the deflection of the impact point is obtained as follows:

$$\omega_O = \frac{K\cdot\delta^{\frac{3}{2}} + K\delta^{\frac{3}{2}}\cdot\frac{8(1-e)}{5e\dot{\delta}^{(-)}}\cdot\dot{\delta}}{6E_2I_2L}\cdot xy\cdot\left(L^2 - x^2 - y^2\right) \tag{11}$$

Under the contact force produced by the impact of rock sphere on metal plate, the energy absorbed by the bending deformation of metal plate W_B is as follows:

$$W_B = \frac{\left[K\cdot\delta^{\frac{3}{2}} + K\delta^{\frac{3}{2}}\cdot\frac{8(1-e)}{5e\dot{\delta}^{(-)}}\cdot\dot{\delta}\right]^2}{12E_2I_2L}\cdot xy\cdot\left(L^2 - x^2 - y^2\right) \tag{12}$$

In the compression stage where the rock sphere conducts elastic-direct impact on the bilateral fixed supporting (define as Working condition 1 or Con 1) metal plate, the initial impact energy is completely converted into the total energy absorbed and consumed by the rock sphere and energy of the bending deflection of the metal plate. Assuming the maximum compression of the rock sphere is $\delta_{\max 1}$ when impacting the bilateral fixed supporting metal plate, and $P_{\max 1}$ is the maximum contact force, m_1 is the mass of the rock sphere, according to the law of conservation of energy:

$$\frac{1}{2}m_1v_1^2 = W_{QZ} + W_B \tag{13}$$

Substitute Eqs. (7) and (12) into Eq. (13) and get that:

$$\frac{1}{2}m_1v_1^2 = \frac{2K}{5e}\cdot\delta_{\max 1}^{\frac{5}{2}} + \frac{K^2\cdot\delta_{\max 1}^3}{12E_2I_2L}\cdot xy\cdot(L^2 - x^2 - y^2) \tag{14}$$

According to recursive solution method, the approximate theoretical solution of Eq. (14) can be solved:

$$\delta_{\max 1}^{\frac{5}{2}} = \frac{m_1v_1^2}{2\left[\frac{2K}{5e} + \frac{K^2\cdot\delta_{\max 1}^{\frac{1}{2}}}{12E_2I_2L}\cdot xy\cdot\left(L^2 - x^2 - y^2\right)\right]} \tag{15}$$

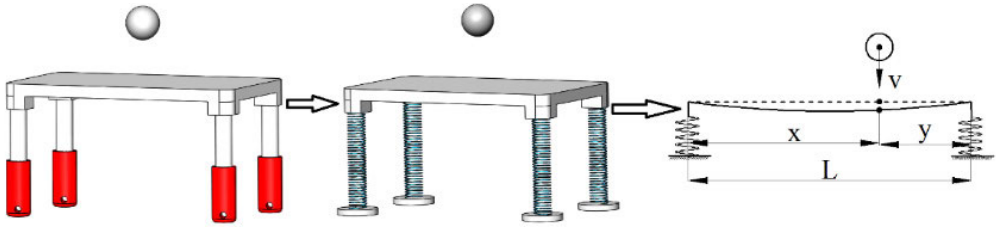

FIGURE 5. Axial direction bending deformation of the metal plate under bilateral elastic supporting.

Define $\delta_{\max 1-0}=0$, then

$$\delta_{\max 1-1}=\left\{\frac{m_1v_1^2}{2\left[\frac{2K}{5e}+\frac{K^2\cdot\delta_{\max 1-0}^{\frac{1}{2}}}{12E_2I_2L}\cdot xy\cdot\left(L^2-x^2-y^2\right)\right]}\right\}^{\frac{2}{5}} \tag{16}$$

$$\delta_{\max 1-2}=\left\{\frac{m_1v_1^2}{2\left[\frac{2K}{5e}+\frac{K^2\cdot\delta_{\max 1-1}^{\frac{1}{2}}}{12E_2I_2L}\cdot xy\cdot\left(L^2-x^2-y^2\right)\right]}\right\}^{\frac{2}{5}} \tag{17}$$

$$\cdots$$

Define the error when the recursive solution stop is $\breve{g}_1$ and the corresponding number of iterations is N, we finally obtain that:

$$\left|\frac{\frac{2K}{5e}\cdot\delta_{\max 1-N}^{\frac{5}{2}}+\frac{K^2\cdot\delta_{\max 1-N}^{3}}{12E_2I_2L}\cdot xy\cdot\left(L^2-x^2-y^2\right)-\frac{1}{2}m_1v_1^2}{\frac{1}{2}m_1v_1^2}\right|\leq\breve{g}_1 \tag{18}$$

$$\delta_{\max 1-N}=\left\{\frac{m_1v_1^2}{2\left[\frac{2K}{5e}+\frac{K^2\cdot\delta_{\max 1-(N-1)}^{\frac{1}{2}}}{12E_2I_2L}\cdot xy\cdot\left(L^2-x^2-y^2\right)\right]}\right\}^{\frac{2}{5}},\quad N\geq 1 \tag{19}$$

The maximum contact force in the condition of the rock sphere impact contact with the bilateral fixed supporting metal plate can be expressed as:

$$P_{\max 1}=K\cdot\left\{\frac{m_1v_1^2}{2\left[\frac{2K}{5e}+\frac{K^2\cdot\delta_{\max 1-(N-1)}^{\frac{1}{2}}}{12E_2I_2L}\cdot xy\cdot\left(L^2-x^2-y^2\right)\right]}\right\}^{\frac{3}{5}} \tag{20}$$

B. DYNAMIC MODEL WHEN THE ROCK SPHERE IMPACTING THE BILATERAL ELASTIC SUPPORTING METAL PLATE

In this paper, we use a spring with certain supporting stiffness to equivalent replace the prop. As shown in Figure 5, in the stage of impact-compression, the contact force between rock sphere and metal plate increases gradually, and it reaches the maximum at the end of critical compression. During the whole process, the compression reaction force of the spring (Prop) is equal to the maximum compression force.

The operating condition is: the four-corner support of constant stiffness spring is arranged to simulate the prop and k_T represents the stiffness, we also just consider the axial bending deformation of the metal plate. According to Eq. (8), it can be calculated that the supporting force at the left and right ends of the metal plate is $F_{z1}=\frac{Py}{L}$ and $F_{z2}=\frac{Px}{L}$ respectively, then the force of every spring on both sides (left spring F_{T1}, right spring F_{T2}) can be shown as follows:

$$\begin{aligned}F_{T1}&=\frac{\left[K\cdot\delta^{\frac{3}{2}}+K\delta^{\frac{3}{2}}\cdot\frac{8(1-e)}{5e\delta^{(-)}}\cdot\dot{\delta}\right]\cdot y}{2L},\\ F_{T2}&=\frac{\left[K\cdot\delta^{\frac{3}{2}}+K\delta^{\frac{3}{2}}\cdot\frac{8(1-e)}{5e\delta^{(-)}}\cdot\dot{\delta}\right]\cdot x}{2L}\end{aligned} \tag{21}$$

The compression length (left spring ω_{T1}, right spring ω_{T2}) is respectively:

$$\begin{aligned}\omega_{T1}&=\frac{\left[K\cdot\delta^{\frac{3}{2}}+K\delta^{\frac{3}{2}}\cdot\frac{8(1-e)}{5e\delta^{(-)}}\cdot\dot{\delta}\right]\cdot y}{2Lk_T},\\ \omega_{T2}&=\frac{\left[K\cdot\delta^{\frac{3}{2}}+K\delta^{\frac{3}{2}}\cdot\frac{8(1-e)}{5e\delta^{(-)}}\cdot\dot{\delta}\right]\cdot x}{2Lk_T}\end{aligned} \tag{22}$$

The absorbed energy by the compression of the spring (F_T refer to F_{T1} and F_{T2}, ω_T refer to ω_{T1} and ω_{T2}) is:

$$\begin{aligned}W_{T1}&=\sum\int F_T d\omega_T\\ &=\frac{\left[K\cdot\delta^{\frac{3}{2}}+K\delta^{\frac{3}{2}}\cdot\frac{8(1-e)}{5e\delta^{(-)}}\cdot\dot{\delta}\right]^2\cdot\left(x^2+y^2\right)}{4L^2k_T}\end{aligned} \tag{23}$$

In the compression stage where the rock sphere conducts elastic-direct impact on the bilateral elastic supporting (define as Working condition 2 or Con 2) metal plate, the impact energy of the rock sphere is completely converted into the total energy absorbed and consumed by the rock

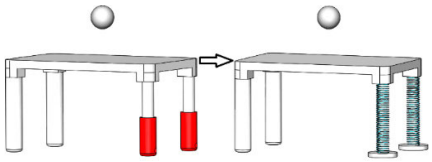

FIGURE 6. Axial direction bending deformation of the unilateral fixed and unilateral elastic supported metal plate.

sphere, energy absorbed by the bending deflection of the metal plate, and energy absorbed by the compression of the bilateral spring. Assuming the maximum compression of the rock sphere is $\delta_{\max 2}$ when impacting the bilateral elastic supporting metal plate, and $P_{\max 2}$ is the maximum contact force, according to the law of conservation of energy:

$$\frac{1}{2}m_1v_1^2 = W_{QZ} + W_B + W_{T1} \tag{24}$$

Substitute Eqs. (7), (12) and (23) into Eq. (24), we can obtain that:

$$\frac{1}{2}m_1v_1^2 = \frac{2K}{5e}\cdot\delta_{\max 2}^{\frac{5}{2}} + \frac{K^2\cdot\delta_{\max 2}^3}{12E_2I_2L}\cdot xy\cdot\left(L^2-x^2-y^2\right) + \frac{K^2\cdot\delta_{\max 2}^3\cdot\left(x^2+y^2\right)}{4L^2k_T} \tag{25}$$

Define the error when the recursive solution stop is $\breve{g}_2$, $F_{T1\max}$ and $F_{T2\max}$ is the maximum force of the left spring and the right spring respectively, we also can solve the Eq. (25) according to recursive solution method that (26)–(30), as shown at the bottom of this page.

C. DYNAMIC MODEL WHEN THE ROCK SPHERE IMPACTING THE UNILATERAL ELASTIC UNILATERAL FIXED SUPPORTED METAL PLATE

The operating condition shown in Figure 6 is that one side (two corners) of the metal plate is set to fixed support while the other side (two corners) is the flexible support by the jack. These two jacks are also equivalent to the spring with the constant stiffness k_T and only the axial bending deformation of the metal plate is considered. At this time, the deformation of the metal plate can be decomposed into two parts: the bending deflection of a cantilever beam and the bending deflection of a simply-supported beam, as shown in Figure 7.

As for the model of simply supported beam: according to the force balance, the sum of F_G(supporting force of the fixed supported end) and F_T (supporting force of the elastic supported end) on both sides is equal to the contact force P. Assuming the distance between the impact point and the end

$$\delta_{\max 2-N} = \left\{\frac{m_1v_1^2}{2\left[\frac{2K}{5e} + \frac{K^2\cdot\delta_{\max 2-(N-1)}^{\frac{1}{2}}}{12E_2I_2L}\cdot xy\cdot\left(L^2-x^2-y^2\right) + \frac{K^2\cdot\delta_{\max 2-(N-1)}^{\frac{1}{2}}\cdot\left(x^2+y^2\right)}{4L^2k_T}\right]}\right\}^{\frac{2}{5}}, \quad N \geq 1 \tag{26}$$

$$\left|\frac{\frac{2K}{5e}\cdot\delta_{\max 2-N}^{\frac{5}{2}} + \frac{K^2\cdot\delta_{\max 2-N}^3}{12E_2I_2L}\cdot xy\cdot\left(L^2-x^2-y^2\right) + \frac{K^2\cdot\delta_{\max 2-N}^3\cdot\left(x^2+y^2\right)}{4L^2k_T} - \frac{1}{2}m_1v_1^2}{\frac{1}{2}m_1v_1^2}\right| \leq \breve{g}_2 \tag{27}$$

$$P_{\max 2} = K\cdot\left\{\frac{m_1v_1^2}{2\left[\frac{2K}{5e} + \frac{K^2\cdot\delta_{\max 2-(N-1)}^{\frac{1}{2}}}{12E_2I_2L}\cdot xy\cdot\left(L^2-x^2-y^2\right) + \frac{K^2\cdot\delta_{\max 2-(N-1)}^{\frac{1}{2}}\cdot\left(x^2+y^2\right)}{4L^2k_T}\right]}\right\}^{\frac{3}{5}} \tag{28}$$

$$F_{T1\max} = K\cdot\left\{\frac{m_1v_1^2}{2\left[\frac{2K}{5e} + \frac{K^2\cdot\delta_{\max 2-(N-1)}^{\frac{1}{2}}}{12E_2I_2L}\cdot xy\cdot\left(L^2-x^2-y^2\right) + \frac{K^2\cdot\delta_{\max 2-(N-1)}^{\frac{1}{2}}\cdot\left(x^2+y^2\right)}{4L^2k_T}\right]}\right\}^{\frac{3}{5}}\cdot\frac{y}{2L} \tag{29}$$

$$P_{T2\max} = K\cdot\left\{\frac{m_1v_1^2}{2\left[\frac{2K}{5e} + \frac{K^2\cdot\delta_{\max 2-(N-1)}^{\frac{1}{2}}}{12E_2I_2L}\cdot xy\cdot\left(L^2-x^2-y^2\right) + \frac{K^2\cdot\delta_{\max 2-(N-1)}^{\frac{1}{2}}\cdot\left(x^2+y^2\right)}{4L^2k_T}\right]}\right\}^{\frac{3}{5}}\cdot\frac{x}{2L} \tag{30}$$

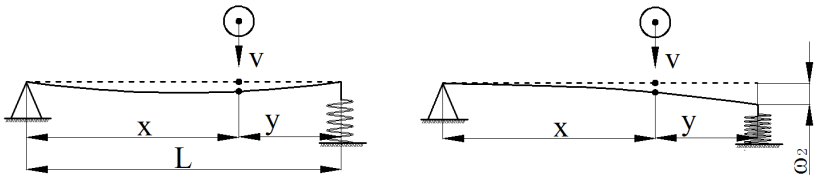

FIGURE 7. Bending deflection of the cantilever beam and the simply-supported beam.

of fixed support is x, it can be obtained:

$$F_G = \frac{\left[K \cdot \delta^{\frac{3}{2}} + K\delta^{\frac{3}{2}} \cdot \frac{8(1-e)}{5e\dot{\delta}^{(-)}} \cdot \dot{\delta}\right] \cdot y}{L},$$
$$F_T = \frac{\left[K \cdot \delta^{\frac{3}{2}} + K\delta^{\frac{3}{2}} \cdot \frac{8(1-e)}{5e\dot{\delta}^{(-)}} \cdot \dot{\delta}\right] \cdot x}{L} \quad (31)$$

At this time, the impact point's bending deflection of the simply-supported beam when the rock sphere impacts the metal plate is obtained as follows:

$$\omega_{11} = \frac{\left[K \cdot \delta^{\frac{3}{2}} + K\delta^{\frac{3}{2}} \cdot \frac{8(1-e)}{5e\dot{\delta}^{(-)}} \cdot \dot{\delta}\right]}{6E_2I_2L} \cdot xy \cdot (L^2 - x^2 - y^2) \quad (32)$$

The deflection-curve equation and the maximum deflection of the cantilever beam are obtained when the concentrated force P acts on the end of the cantilever beam (ω is the deflection of the point in the metal plate, $\omega_{\max}$ is the maximum deflection of the metal plate):

$$\begin{cases} E_L I\omega = -\frac{Px^2}{6} \cdot (3L - x) \\ \omega_{\max} = \frac{PL^3}{3E_L I} \end{cases} \quad (33)$$

The force F_T is applied vertically to the spring supporting end. As for the model of a cantilever beam supported by the spring on one side, the maximum deflection occurs at the end point. Assuming the deflection value is ω_2, and combining with Eq. (33), it can be seen that:

$$\omega_2 = \frac{(F_T - F_k) L^3}{3E_2I_2} \quad (34)$$

For the spring, the total spring force

$$F_k = 2F_{kT} = 2k_T \cdot \omega_2 = 2k_T \cdot \frac{(F_T - F_k) L^3}{3E_2I_2} \quad (35)$$

According to Eq. (34) and (35),

$$F_k = \frac{F_T}{1 + \frac{3E_2I_2}{2k_TL^3}} = \frac{2k_TL^2\left[K \cdot \delta^{\frac{3}{2}} + K\delta^{\frac{3}{2}} \cdot \frac{8(1-e)}{5e\dot{\delta}^{(-)}} \cdot \dot{\delta}\right] \cdot x}{2k_TL^3 + 3E_2I_2} \quad (36)$$

Combine with Eq. (31) and (35),

$$\omega_2 = \frac{\left[K \cdot \delta^{\frac{3}{2}} + K\delta^{\frac{3}{2}} \cdot \frac{8(1-e)}{5e\dot{\delta}^{(-)}} \cdot \dot{\delta}\right] \cdot xL^2}{2k_TL^3 + 3E_2I_2} \quad (37)$$

Assuming ω_2 represents the equivalent force F_{DX}, the maximum deflection produced at the end of the cantilever beam shows:

$$\omega_2 = \frac{\left[K \cdot \delta^{\frac{3}{2}} + K\delta^{\frac{3}{2}} \cdot \frac{8(1-e)}{5e\dot{\delta}^{(-)}} \cdot \dot{\delta}\right] \cdot xL^2}{2k_TL^3 + 3E_2I_2} = \frac{F_{DX}L^3}{3E_2I_2} \quad (38)$$

$$F_{DX} = \frac{3E_2I_2\left[K \cdot \delta^{\frac{3}{2}} + K\delta^{\frac{3}{2}} \cdot \frac{8(1-e)}{5e\dot{\delta}^{(-)}} \cdot \dot{\delta}\right] \cdot x}{L\left(2k_TL^3 + 3E_2I_2\right)} \quad (39)$$

The impact point's bending deflection of the cantilever beam when the rock sphere impacts the metal plate can be seen as follows:

$$\omega_{12} = \frac{\left[K \cdot \delta^{\frac{3}{2}} + K\delta^{\frac{3}{2}} \cdot \frac{8(1-e)}{5e\dot{\delta}^{(-)}} \cdot \dot{\delta}\right] \cdot x^3}{2L\left(2k_TL^3 + 3E_2I_2\right)} \cdot (3L - x) \quad (40)$$

The impact point's total bending deflection when the rock sphere impacts the metal plate can be seen as follows:

$$\begin{aligned} \omega_1 &= \omega_{11} + \omega_{12} \\ &= \frac{\left[K \cdot \delta^{\frac{3}{2}} + K\delta^{\frac{3}{2}} \cdot \frac{8(1-e)}{5e\dot{\delta}^{(-)}} \cdot \dot{\delta}\right]}{6E_2I_2L} \cdot xy \cdot (L^2 - x^2 - y^2) \\ &\quad + \frac{\left[K \cdot \delta^{\frac{3}{2}} + K\delta^{\frac{3}{2}} \cdot \frac{8(1-e)}{5e\dot{\delta}^{(-)}} \cdot \dot{\delta}\right] \cdot x^3}{2L(2k_TL^3 + 3E_2I_2)} \cdot (3L - x) \end{aligned} \quad (41)$$

In the process, the energy is transformed into three parts: the energy W_J of the elastic deformation of a simply supported beam, the energy W_T of the elastic deformation of spring compression, and the energy W_X of the elastic deformation of a cantilever beam. And the calculated equations are shown as the follow:

$$\begin{aligned} W_J &= \int P d\omega_{11} \\ &= \frac{\left[K \cdot \delta^{\frac{3}{2}} + K\delta^{\frac{3}{2}} \cdot \frac{8(1-e)}{5e\dot{\delta}^{(-)}} \cdot \dot{\delta}\right]^2}{12E_2I_2L} \cdot xy \cdot (L^2 - x^2 - y^2) \end{aligned} \quad (42)$$

$$\begin{aligned} W_T &= 2\int \frac{F_K}{2} d\omega_2 \\ &= \frac{k_TL^4\left[K \cdot \delta^{\frac{3}{2}} + K\delta^{\frac{3}{2}} \cdot \frac{8(1-e)}{5e\dot{\delta}^{(-)}} \cdot \dot{\delta}\right]^2 \cdot x^2}{(2k_TL^3 + 3E_2I_2)^2} \end{aligned} \quad (43)$$

$$\begin{aligned} W_X &= \int F_{DX} d\omega_2 \\ &= \frac{3E_2I_2\left[K \cdot \delta^{\frac{3}{2}} + K\delta^{\frac{3}{2}} \cdot \frac{8(1-e)}{5e\dot{\delta}^{(-)}} \cdot \dot{\delta}\right]^2 \cdot x^2L}{(2k_TL^3 + 3E_2I_2)^2} \end{aligned} \quad (44)$$

In the compression stage where the rock sphere conducts elastic-direct impact on the unilateral fixed and unilateral elastic supported (define as Working condition 3 or Con 3) metal plate, the impact energy of the rock sphere is completely converted into four parts: the total energy absorbed and consumed by the rock sphere, energy absorbed by the bending deformation of the simply-supported beam W_J, energy absorbed by the elastic deformation of the spring W_T and energy absorbed by the bending deformation of the cantilever beam W_X. Assuming the maximum compression of the rock sphere is δ_{max3} when impacting the unilateral elastic unilateral fixed supported metal plate, and P_{max3} is the maximum contact force, according to the law of conservation of energy:

$$\frac{1}{2}m_1v_1^2 = W_{QZ} + W_J + W_T + W_X \tag{45}$$

Substitute Eqs. (7), (42), (43) and (44) into Eq. (45), we obtain that:

$$\frac{1}{2}m_1v_1^2 = \frac{2K}{5e}\cdot\delta_{\max 5}^{\frac{5}{2}} + \frac{K^2\cdot\delta_{\max 3}^3}{12E_2I_2L}\cdot xy\cdot(L^2-x^2-y^2) + \frac{k_TL^4K^2\cdot\delta_{\max 3}^3\cdot x^2}{(2k_TL^3+3E_2I_2)^2} + \frac{3E_2I_2K^2\cdot\delta_{\max 3}^3\cdot x^2L}{(2k_TL^3+3E_2I_2)^2} \tag{46}$$

Define the error when the recursive solution stop is $\breve{g}_3$, Eq. (46) can be solved according to recursive solution method that (47)–(50), as shown at the bottom of this page.

III. YIELD VELOCITY MODEL WHEN THE ROCK IMPACTING THE DIFFERENT SUPPORTING FORM METAL PLATE

According to the Drucker-Prager criterion [56]–[61] and references [43], [62], [63], the critical yield deformation of the rock is:

$$\delta_{my} = \left[\frac{2\pi Rk}{K(6\Theta_1+\sqrt{3}\Theta_2)}\right]^2 \tag{51}$$

where $k = \frac{6\cos\varphi}{\sqrt{3}(3-\sin\varphi)}$, $\alpha = \frac{2\sin\varphi}{\sqrt{3}(3-\sin\varphi)}$, $\Theta_1 = \alpha(1+\mu_1)(1-\varepsilon_0\tan^{-1}\frac{1}{\varepsilon_0})$, $\Theta_2 = -(1+\mu_1)(1-\varepsilon_0\tan^{-1}\frac{1}{\varepsilon_0})+\frac{3}{2}(1+\varepsilon_0^2)^{-1}$, $\varepsilon_0 = 0.3824 - 1.181\alpha + 0.3307\mu_1 + 0.4646\alpha^2 - 1.083\alpha\cdot\mu_1 - 0.007665\mu_1^2 - 3.35\alpha^3 + 0.2447\alpha^2\cdot\mu_1 - 0.05763\alpha\cdot\mu_1^2 + 0.0101\mu_1^3$.

On the Basis of the Drucker-Prager yield criterion, and combine with Eqs. (14), (25) and (46), the critical yield velocities of rock sphere under the bilateral fixed supporting v_{y1}, the bilateral elastic supporting v_{y2}, and the unilateral elastic unilateral fixed supporting v_{y3} are obtained as in (52)–(54), as shown at the top of the next page.

$$\delta_{\max 3-N} = \left\{\frac{m_1v_1^2}{2\left[\frac{2K}{5e} + \frac{K^2\cdot\delta_{\max 3-(N-1)}^{\frac{1}{2}}}{12E_2I_2L}\cdot xy\cdot(L^2-x^2-y^2) + \frac{k_TL^4K^2\cdot\delta_{\max 3-(N-1)}^{\frac{1}{2}}\cdot x^2}{(2k_TL^3+3E_2I_2)^2} + \frac{3E_2I_2K^2\cdot\delta_{\max 3-(N-1)}^{\frac{1}{2}}\cdot x^2L}{(2k_TL^3+3E_2I_2)^2}\right]}\right\}^{\frac{2}{5}}, \quad N\geq 1 \tag{47}$$

$$\left|\frac{\frac{2K}{5e}\cdot\delta_{\max 3-N}^{\frac{5}{2}} + \frac{K^2\cdot\delta_{\max 3-N}^3}{12E_2I_2L}\cdot xy\cdot(L^2-x^2-y^2) + \frac{k_TL^4K^2\cdot\delta_{\max 3-N}^3\cdot x^2}{(2k_TL^3+3E_2I_2)^2} + \frac{3E_2I_2K^2\cdot\delta_{\max 3-N}^3\cdot x^2L}{(2k_TL^3+3E_2I_2)^2} - \frac{1}{2}m_1v_1^2}{\frac{1}{2}m_1v_1^2}\right| \leq \breve{g}_3 \tag{48}$$

$$P_{\max 3} = K\cdot\left\{\frac{m_1v_1^2}{2\left[\frac{2K}{5e} + \frac{K^2\cdot\delta_{\max 3-(N-1)}^{\frac{1}{2}}}{12E_2I_2L}\cdot xy\cdot(L^2-x^2-y^2) + \frac{k_TL^4K^2\cdot\delta_{\max 3-(N-1)}^{\frac{1}{2}}\cdot x^2}{(2k_TL^3+3E_2I_2)^2} + \frac{3E_2I_2K^2\cdot\delta_{\max 3-(N-1)}^{\frac{1}{2}}\cdot x^2L}{(2k_TL^3+3E_2I_2)^2}\right]}\right\}^{\frac{3}{5}} \tag{49}$$

$$F_{kT\max} = \frac{k_TL^2\cdot x}{2k_TL^3+3E_2I_2}\cdot K\cdot\left\{\frac{m_1v_1^2}{2\left[\frac{2K}{5e} + \frac{K^2\cdot\delta_{\max 3-(N-1)}^{\frac{1}{2}}}{12E_2I_2L}\cdot xy\cdot(L^2-x^2-y^2) + \frac{k_TL^4K^2\cdot\delta_{\max 3-(N-1)}^{\frac{1}{2}}\cdot x^2}{(2k_TL^3+3E_2I_2)^2} + \frac{3E_2I_2K^2\cdot\delta_{\max 3-(N-1)}^{\frac{1}{2}}\cdot x^2L}{(2k_TL^3+3E_2I_2)^2}\right]}\right\}^{\frac{3}{5}} \tag{50}$$

$$v_{y1} = \sqrt{\frac{2}{m_1} \cdot \left[\frac{2K}{5e} \cdot \delta_{my}^{\frac{5}{2}} + \frac{K^2 \cdot \delta_{my}^3}{12E_2I_2L} \cdot xy \cdot (L^2 - x^2 - y^2) \right]} \tag{52}$$

$$v_{y2} = \sqrt{\frac{2}{m_1} \cdot \left[\frac{2K}{5e} \cdot \delta_{my}^{\frac{5}{2}} + \frac{K^2 \cdot \delta_{my}^3}{12E_2I_2L} \cdot xy \cdot (L^2 - x^2 - y^2) + \frac{K^2 \cdot \delta_{my}^3 \cdot (x^2 + y^2)}{4L^2k_T} \right]} \tag{53}$$

$$v_{y3} = \sqrt{\frac{2}{m_1} \left[\frac{2K}{5e} \cdot \delta_{my}^{\frac{5}{2}} + \frac{K^2 \cdot \delta_{my}^3}{12E_2I_2L} \cdot xy \cdot (L^2 - x^2 - y^2) + \frac{k_T L^4 K^2 \cdot \delta_{my}^3 \cdot x^2}{(2k_T L^3 + 3E_2I_2)^2} + \frac{3E_2I_2K^2 \cdot \delta_{my}^3 \cdot x^2 L}{(2k_T L^3 + 3E_2I_2)^2} \right]} \tag{54}$$

IV. RESULTS DISCUSSION AND ANALYSIS

During the mining of top-coal caving, coal gangue falls and accumulates on the overlying strata metal plate which is in the tail beam of the hydraulic support. During the process, the impact-contact between the coal or gangue particles and the metal plate occurs, which will cause the vibration response of the tail beam. Based on the theoretical model when the rock sphere elastic impact on the various supported metal plate established in this paper, a kind of coal gangue and metal plate is respectively selected and regarded as the research object, which the material properties and the size of the sphere particles and the plate are shown in Table 1, and the influence about the elastic support, the spring stiffness and the length of the metal plate on the system dynamic response and the response differences when the coal gangue impacting the metal plate were analyzed respectively.

According to Table 1 and Eqs. (3) and (4), the contact stiffness when the coal gangue respectively impact on the metal plate can be calculated, $K_{Coal} = 5.11545 \times 10^8$ N/m$^{1.5}$, $K_{Gangue1} = 3.10405 \times 10^9$ N/m$^{1.5}$, $K_{Gangue2} = 3.40396 \times 10^9$ N/m$^{1.5}$. Take the restitution coefficient e = 0.65.

A. EFFECTS OF THE ELASTIC SUPPORT AND THE IMPACT POSITION TO THE YIELD VELOCITY AND THE CONTACT RESPONSES

1) EFFECTS OF THE ELASTIC SUPPORTING AND THE IMPACT POSITION TO THE YIELD VELOCITY

Define the spring stiffness $k_{TD} = K_{Coal} = 5.11545 \times 10^8$ N/m$^{1.5}$. According to the material parameters in Table 1, when the Coal-Rock sphere and the Gangue-Rock sphere 1impact on the any axial position of the metal plate, the rock yield velocity under the bilateral fixed support (No elastic support), the bilateral fixed support and the unilateral elastic unilateral fixed support are shown in Figures 8-9.

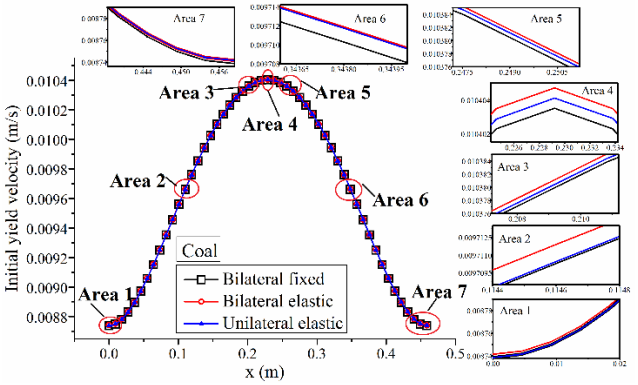

FIGURE 8. Initial velocity of the coal.

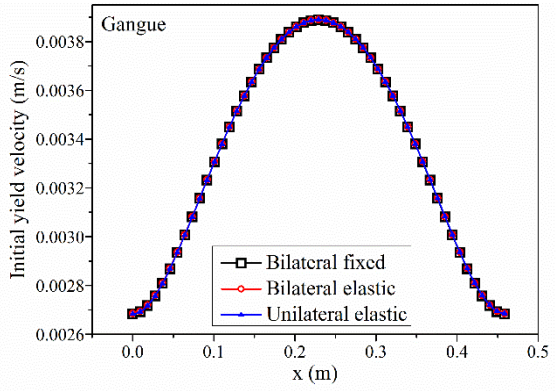

FIGURE 9. Initial velocity of the gangue.

From the figures, when $k_{TD} = K_{Coal} = 5.11545 \times 10^8$ N/m$^{1.5}$, with the impact position changes from the left end of the metal plate to the right end, yield velocities of the Coal-Rock sphere and the Gangue-Rock sphere 1 all appear

TABLE 1. Calculated parameters of Coal-rock sphere impact the metal plate.

Contact body	ρ_i/kg.m^{-3}	E_i/GPa	μ_i	ζ/MPa	ϕ/(°)	R/mm	L/mm	B/mm	h/mm
Coal-Rock sphere	1380	2.26	0.28	8.39	25	25	--	--	--
Gangue-Rock sphere 1	2400	16	0.28	37.68	37	20.7888	--	--	--
Gangue-Rock sphere 2	2400	16	0.28	37.68	37	25	--	--	--
Metal plate	7850	210	0.3	--	--	--	458.4	360	8

TABLE 2. Coal gangue initial yield velocity of the impact point in the selected areas.

Coal-Rock sphere							
	Area 1 0.013752	**Area 2** 0.1146	**Area 3** 0.210864	**Area 4** 0.2292	**Area 5** 0.247536	**Area 6** 0.3438	**Area 7** 0.449232
v_{y1}	0.00876323	0.009710283	0.010383947	0.010403508	0.010383947	0.009710283	0.008749759
v_{y2}	0.00876592	0.009711894	0.01038516	0.010404711	0.01038516	0.009711894	0.008752507
v_{y3}	0.008763232	0.009710444	0.010384457	0.01040411	0.01038465	0.009711733	0.008752506
Gangue-Rock sphere 1							
	Area 1 0.013752	**Area 2** 0.1146	**Area 3** 0.210864	**Area 4** 0.2292	**Area 5** 0.247536	**Area 6** 0.3438	**Area 7** 0.449232
v_{y1}	0.002703202	0.003414581	0.003876427	0.003889453	0.003876427	0.003414581	0.002692325
v_{y2}	0.00270537	0.00341572	0.003877236	0.003890253	0.003877236	0.00341572	0.002694546
v_{y3}	0.002703204	0.003414695	0.003876767	0.003889853	0.003876896	0.003415606	0.002694545

the approximate parabola form which increases first and then decreases. The rock minimum yield velocity appears at the left end of the plate (or appears at the both ends together), while the position where the maximum yield velocity appears close to the axial midpoint of the metal plate. The yield velocity when the Coal-Rock sphere impact on the metal plate is larger than 0.0087m/s, but the yield velocity of the Gangue-Rock sphere 1 is in the range of 0.00268m/s to 0.0039m/s. When the same spherical rock impact on the same position of the three different support form metal plate, the rock yield velocity is very similar. But there are still differences in the rock yield velocity when the same spherical rock impact on the same position of the different support form metal plate due to the exist of the elastic support.

To make a clear comparison, taking the yield velocity when the coal impact on the metal plate as the example. Seven different axial positions of the metal plate were respectively selected and defined as Area 1 to Area 7, which the impact points were selected according to the advance from the left end of the metal plate to the right end. Regional impact velocity under three different supporting forms is shown in Figure 8. The initial yield velocity of the chosen impact point in the seven regional coordinate intervals shown in Figure 8 when the coal gangue particle impacting the metal plate is shown in Table 2 (The length of the metal plate is 0.4584m. It divides into 100 portions, each of which is 0.004584m).

From Figures 8-9 and Table 2, according to Area 1, when the particle impact close to the left end of the metal plate, the rock yield velocity curves of the bilateral fixed support and the unilateral elastic unilateral fixed support almost exactly, the reason is that the left end of the metal plate in the above two conditions are both fixed support. According to Area 7, when the particle impact close to the right end of the metal plate, the rock yield velocity curves of the bilateral elastic support and the unilateral elastic unilateral fixed support also almost exactly, the reason is that the right end of the metal plate in the above two conditions are both elastic support. Observe the Areas 1-7, the rock yield velocity is the minimum when impacting the bilateral fixed supporting metal plate, while the rock yield velocity is the maximum when impacting the bilateral elastic supporting metal plate. The rock yield velocity is between the above mentioned two conditions when impacting the unilateral elastic unilateral fixed support metal plate. It can be seen that the elastic support at the end of the metal plate when the spherical rock impact the metal plate will increase the rock initial yield velocity. In addition, when advancing from Area 1 to Area 7, the critical yield velocity of the rock under the unilateral elastic unilateral fixed support condition is gradually close to that under the bilateral elastic supporting condition, while gradually far away from that under the bilateral fixed support condition.

2) EFFECTS OF THE ELASTIC SUPPORTING AND THE IMPACT POSITION TO THE SYSTEM CONTACT RESPONSE

According to the material parameters in Table 1, take the impact velocity when the Coal-Rock sphere impact on the metal plate is 0.008m/s. The system maximum contact force, the rock maximum compression deformation, the maximum deflection of the metal plate impact point, the spring response force and the system energy conversion ratio when the coal gangue impact on the any axial position of the bilateral fixed support, the bilateral elastic support and the unilateral elastic unilateral fixed support metal plate are obtained, as is shown in Figure 10 (1)-(8), respectively.

From the figures, with the impact point advance from the left end of the metal plate to the right end, the contact force, the rock compression deformation, the ratio of the total energy absorbed and consumed by the rock sphere, and the ratio of the total energy absorbed by the rock sphere all appear the trend which decreases first and then increases. The minimum value of the above responses is close to the axial midpoint of the metal plate. The impact point deflection of the metal plate and the ratio of the energy absorbed by the bending deformation of the metal plate both appear the trend which increases first and then decreases. The minimum value of these two responses is also close to the axial midpoint of the metal plate. The left end spring force when impact the bilateral elastic support metal plate presents the decreases trend, while its right end spring force and the spring force when impact the unilateral elastic unilateral fixed support metal plate both present the increase trend. The ratio of the energy absorbed by the spring under the bilateral elastic

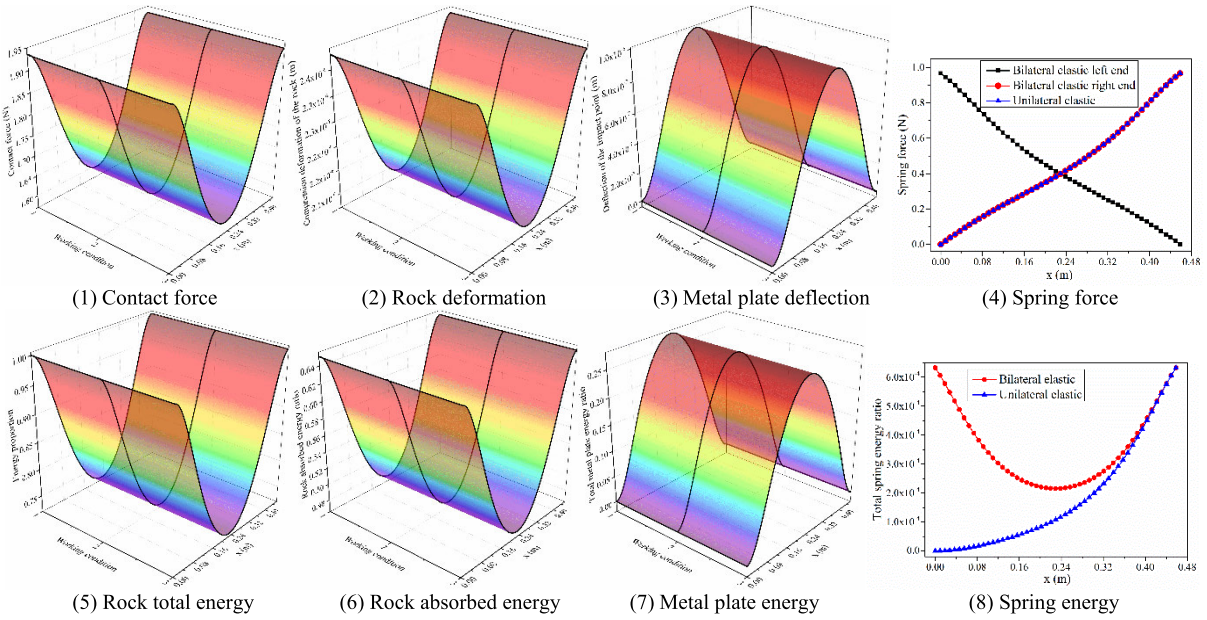

(1) Contact force (2) Rock deformation (3) Metal plate deflection (4) Spring force

(5) Rock total energy (6) Rock absorbed energy (7) Metal plate energy (8) Spring energy

FIGURE 10. The system contact response when the supporting condition and the impact position changes.

TABLE 3. Part of the system maximum contact response when coal impact.

	Contact force (N)			Rock deformation (10^{-6}m)			Metal plate deflection (10^{-7}m)		
	Con 1	Con 2	Con 3	Con 1	Con 2	Con 3	Con 1	Con 2	Con 3
No.1	1.934765	1.934031	1.934765	2.42752	2.426906	2.42752	0	0	0
No.2	1.596266	1.596071	1.596168	2.1354079	2.135234	2.135321	9.930872	9.929656	9.932702
No.3	1.934765	1.934031	1.934031	2.42752	2.426906	2.426906	0	0	1.890195
	Rock total energy ratio			Rock absorbed energy ratio			Metal plate energy ratio		
	Con 1	Con 2	Con 3	Con 1	Con 2	Con 3	Con 1	Con 2	Con 3
No.1	1	0.999367	1	0.65	0.649589	0.65	0	0	0
No.2	0.725764	0.725615	0.725689	0.471746	0.47165	0.471698	0.2742364	0.274169	0.274203
No.3	1	0.999367	0.999367	0.65	0.649589	0.649589	0	0	0

support decreases first and then increases, while the energy absorbed by the spring under the unilateral elastic unilateral fixed support presents the increases trend.

We can also learn from the figures that when the same coal-rock like sphere impact on the same point of the bilateral elastic support metal plate and the unilateral elastic unilateral fixed support metal plate, the left end spring force when impact the bilateral elastic support metal plate has the obvious differences with its right end spring force and with the spring force when impact the unilateral elastic unilateral fixed support metal plate. And the ratio of the energy absorbed by the spring under the bilateral elastic support is larger than that of the unilateral elastic unilateral fixed support. When the same spherical rock impact the three different support form metal plate, the values of the maximum contact force, the maximum rock compression deformation, the impact point maximum deflection of the metal plate, the rock total energy ratio, the ratio of the energy absorbed by the rock, and the ratio of the energy absorbed by the metal plate are similar without the significant differences. The minimum value of the maximum contact force, the maximum rock compression deformation, the impact point maximum deflection of the metal plate, the rock total energy ratio, the ratio of the energy absorbed by the rock, and the maximum value of the energy ratio absorbed by the metal plate all are close to the axial midpoint of the metal plate.

Extract the system maximum contact responses such as the contact force, the rock compression deformation, the impact point deflection of the metal plate, the ratio of the total energy absorbed and consumed by the rock, the ratio of the energy absorbed by the rock and the ratio of the energy absorbed by the metal plate when the impact position is $x = 0$ (Point 1), $x = L/2 = 0.2292$ (Point 2), $x = L = 0.4584$ (Point 3) respectively, as shown in Table 3.

From Table 3, due to the exist of the fixed support in metal plate left end under the bilateral fixed support and the unilateral elastic and unilateral fixed support, the contact responses when impact the left end of the bilateral fixed support and unilateral elastic and unilateral fixed support metal plate are the same. Due to the exist of the elastic support in metal plate right end under the bilateral elastic support and the unilateral elastic and unilateral fixed support, the contact

TABLE 4. Maximum spring force when coal impact (N).

Bilateral elastic left end			Bilateral elastic right end			Unilateral elastic and unilateral fixed		
Point 1	Point 2	Point 3	Point 1	Point 2	Point 3	Point 1	Point 2	Point 3
0.967015	0.399018	0	0	0.399018	0.967015	0	0.399003	0.96692

responses when impact the right end of the bilateral elastic support and unilateral elastic and unilateral fixed support metal plate are the same. When impact on the midpoint of the metal plate, the maximum contact force, the rock compression deformation, the impact point deformation of the metal plate, the ratio of the total energy absorbed and consumed by the rock, the ratio of the energy absorbed by the rock, and the ratio of the energy absorbed by the metal plate all appear the phenomenon which is maximum when impact the bilateral fixed support, take second place when impact the unilateral elastic and unilateral fixed support, minimum when impact the bilateral fixed support. It can be seen that the presence of the spring support will reduce the six contact responses shown in Table 3.

Extract the both ends spring forces of the bilateral elastic support and the spring force of the unilateral elastic unilateral fixed support, as shown in Table 4. When impact on the both ends and the axial midpoint of the metal plate, the spring force under bilateral elastic support is larger than that of the unilateral elastic unilateral fixed support condition. Thus, the increase of the spring support end will reduce the system spring force.

B. EFFECTS OF THE SPRING STIFFNESS TO THE YIELD VELOCITY AND THE SYSTEM CONTACT RESPONSE

Since the elastic support is not involved, the spring stiffness has no effect on the spherical rock impact yield velocity and the contact responses when the rock impact on the bilateral fixed support (No elastic support) metal plate. Define the spring stiffness k_{TD} respectively is [5×10^4, 2.50025×10^8, 5×10^8] N/m$^{1.5}$ respectively. According to the material parameters in Table 1, when Coal-Rock sphere impact on the metal plate, the initial yield velocity curves when the any axial position of the bilateral elastic support and the unilateral elastic unilateral fixed support metal plate is impact are shown in Figures. 11-12.

From the figures, with the increase of the spring stiffness, when impact at the same position of the metal plate, the rock yield velocity under the two different support forms both decrease. Compare with the larger order of magnitude spring stiffness ($\times 10^8$ N/m$^{1.5}$), the shape of the yield velocity curve changes when the spring stiffness is small.

Take the velocity of the Coal-Rock sphere is 0.008m/s which is within its yield velocity range, the system maximum contact force, the rock maximum compression deformation, the impact point maximum deflection of the metal plate, the spring response force and the system energy conversion ratio are obtained when Coal-Rock sphere impact on the any axial position of the bilateral elastic support and the

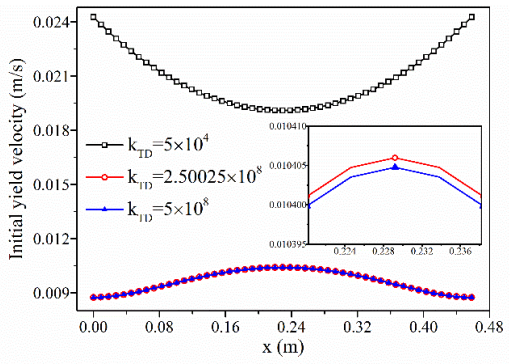

FIGURE 11. Bilateral elastic support.

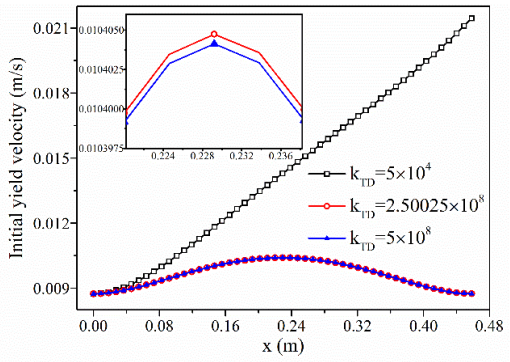

FIGURE 12. Unilateral elastic unilateral fixed support.

unilateral elastic unilateral fixed support metal plate under three different spring stiffness, as shown in Figure 13 (1)-(8) respectively.

When impact at the same velocity, with the changes of the impact position, the shape of the contact responses curves when the spring stiffness is 5×10^4N/m$^{1.5}$ of the bilateral elastic support and the unilateral elastic unilateral fixed support changes compared with which the spring stiffness is 2.50025×10^8 N/m$^{1.5}$ and 5×10^8 N/m$^{1.5}$ respectively. But for both conditions, when the rock impact on the same position of the metal plate, with the increase of the spring stiffness, the maximum contact force, the maximum compression deformation of the rock, the maximum spring force, the maximum ratio of the total energy absorbed and consumed by the rock, and the maximum ratio of the energy absorbed by the rock all increase, while the maximum ratio of the energy absorbed by the spring decline. The impact point maximum deflection of the metal plate and the ratio of the energy absorbed by the metal plate under the bilateral elastic support gradually increase with the increase of the spring

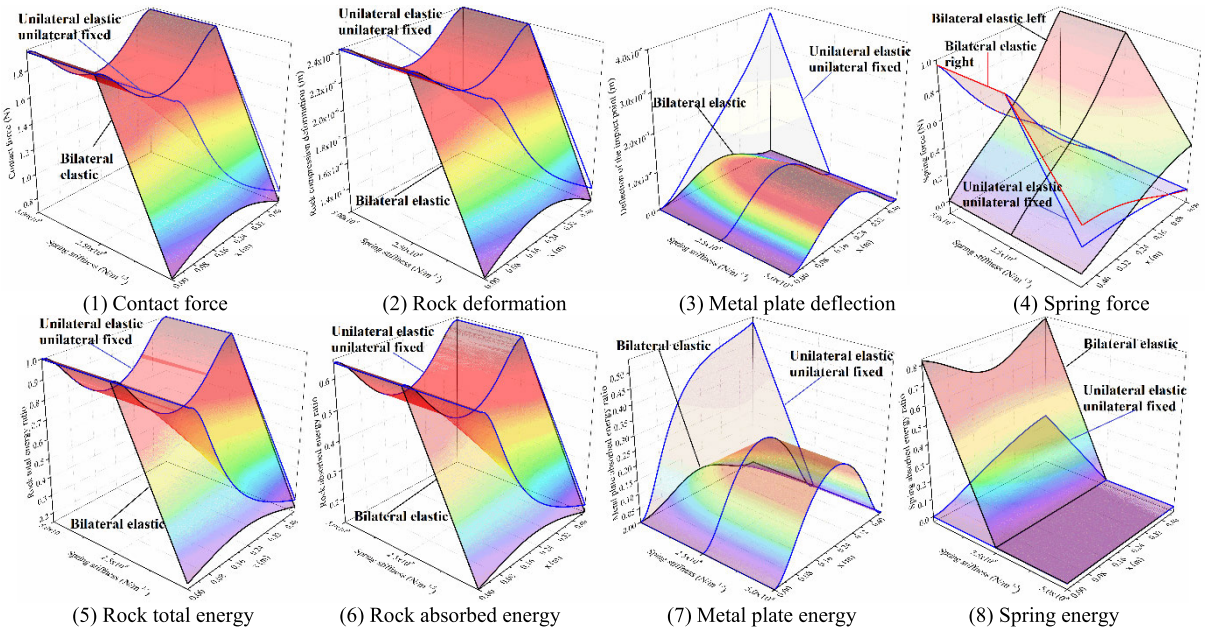

FIGURE 13. The system contact response when the spring stiffness changes.

stiffness. However, due to the impact point maximum deflection of the metal plate under the unilateral elastic unilateral fixed support are composed by the deflection of the simply supported beam and the deflection of the cantilever beam, and the energy absorbed by the metal plate are composed by the energy W_J of the elastic deformation of a simply supported beam and the energy W_X of the elastic deformation of a cantilever beam, the changing trend of the impact point deflection and the energy ratio absorbed by the metal plate when the spring stiffness changes is different from that of the bilateral elastic support. With the increase of the stiffness, the impact point deflection of the metal plate under the unilateral elastic unilateral fixed support decreases gradually. The ratio of the energy W_J absorbed by the elastic deformation of the simply supported beam increases gradually, but the energy W_X absorbed by the elastic deformation of the cantilever beam decreases gradually, after the superposition of the above two part of the energy, the ratio of the total energy absorbed by the metal plate under the unilateral elastic unilateral fixed support decreases first and then increases with the increase of the spring stiffness. It can be seen from the analysis that with the increase of spring stiffness, the energy transformed to the spherical rock from the system increases relatively, while the energy transformed to the spring decreases relatively.

C. EFFECTS OF THE METAL PLATE LENGTH TO THE SYSTEM CONTACT RESPONSE

When k_T is $5\times10^6 N/m^{1.5}$ and the three different support form metal plate is impact, the minimum yield velocity of the coal-rock sphere is larger than 0.0087m/s. Take the impact velocity is 0.008m/s, the system maximum contact force, the rock maximum compression deformation, the impact point maximum deflection of the metal plate, the spring response force and the system energy conversion ratio when coal-rock sphere impact the any axial position of the bilateral fixed support, the bilateral elastic support and the unilateral elastic unilateral fixed support metal plate are obtained, as shown in Figures 14-16.

The length of the metal plate affects the magnitude of the both ends supporting force, the bending deflection under the load and the energy absorbed by the bending deflection of the metal plate. By Figure 14 (1)-(6), three kinds of working conditions, when impact the same point of the metal plate with same velocity from the left end to the right end, with the increase of the metal plate length, the system maximum contact force, the maximum compression deformation of the spherical rock, the ratio of the total energy absorbed and consumed by the rock as well as the ratio of the energy absorbed by the rock gradually decrease, while the impact point maximum deflection of the metal plate and the ratio of the energy absorbed by the metal plate increase gradually. The reason is that the increase in the length of the metal plate reduces its ability to resist its own bending deformation under the action of the external forces, which makes the metal plate more prone to bending and thus makes the metal plate become ''soft and flexible'', so that reducing the ''contact force'' when impact by the same rock.

It can be seen from Figures 15-16 that when the Coal-rock sphere impacting the same point of the metal plate with the same velocity, with the increase of the metal plate length, the spring force at the left end of bilateral elastic support state increases gradually, while the spring force at its right end decreases gradually. The reason is that when the metal

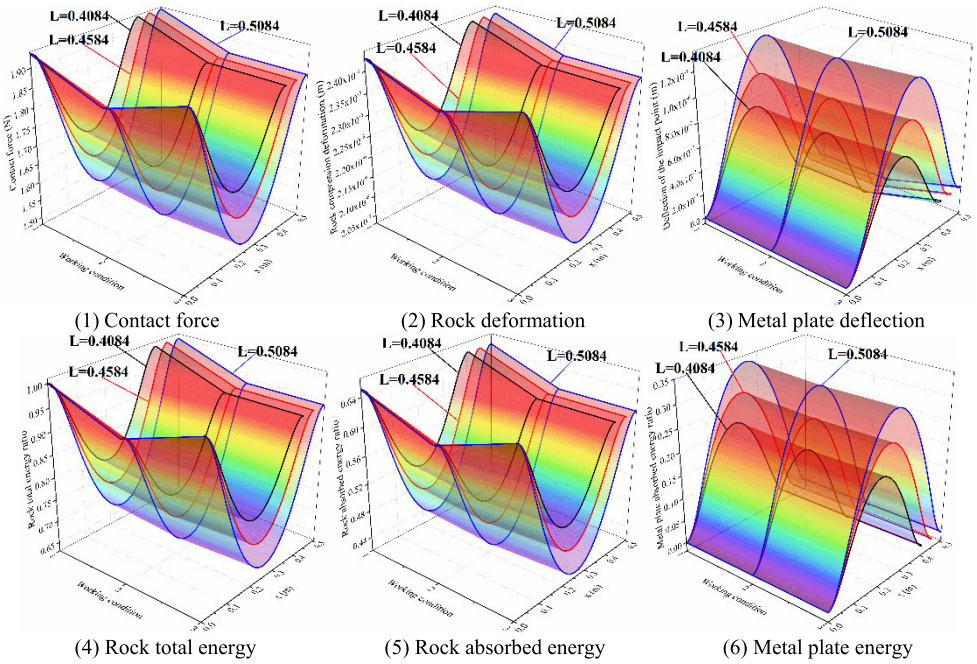

FIGURE 14. The system contact response when the length of the metal plate changes.

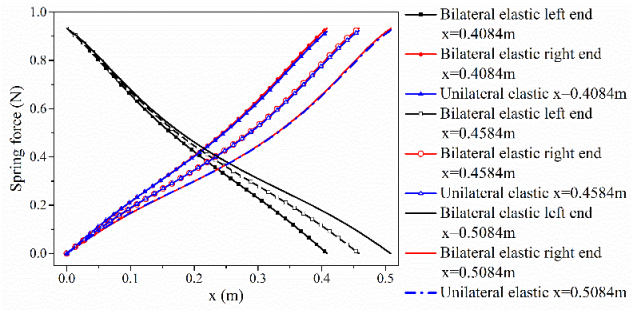

FIGURE 15. Spring force.

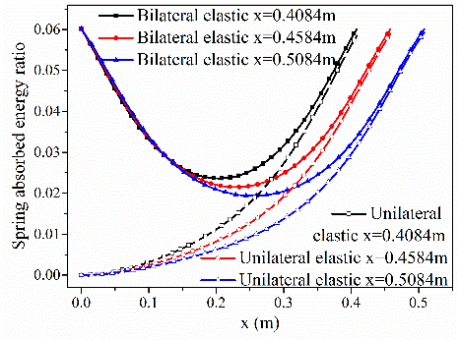

FIGURE 16. Spring energy.

plate is impacted at the same point, with the increase of the metal plate length, the distance between the impact point and the right end of the metal plate increases, meanwhile x/L increases while y/L decreases. Therefore, the proportion of the system total supporting force distributed to the spring at the left end of the metal plate increases. However, with the increase of the metal plate length, the proportion of the total energy absorbed by the spring in the state of the bilateral elastic support increases first and then decreases. When the impact point is close to the left end of the metal plate, it increases gradually with the increase of the metal plate length. When the impact point continues to the right end, it decreases gradually with the increase of the metal plate length.

When the Coal-rock sphere impacting the same point of the metal plate with the same velocity, with the increase of the metal plate length, the spring force and the energy ratio absorbed by the spring in the state of unilateral elastic unilateral fixed support both decrease gradually.

D. EFFECTS OF THE ELASTIC SUPPORT TO THE COAL GANGUE IMPACT CONTACT RESPONSE DIFFERENCES

Because of the different properties of the coal gangue, the contact mechanism and contact response are different when the metal plate is impacted. Define the spring stiffness $k_{TD} = K_{Coal} = 5.11545 \times 10^8$ N/m$^{1.5}$, the dynamic responses of the same mass and volume coal gangue impact the metal plates were analyzed.

According to Tables 1 and Eqs. (52)-(54), the minimum yield velocity of the particles under different conditions are shown in Table 5.

From Table 5, the minimum yield velocity of the selected coal in the paper is above 3 times of the gangue. When impacting the metal plate, the selected gangue in this paper is easier to reach the critical point of the elastic zone than

TABLE 5. Minimum initial yield velocity when coal gangue impact on the metal plate (m/s).

Impact body	v_{y1}	v_{y2}	v_{y3}
Coal-Rock sphere	0.008739	0.008741	0.008739
Gangue-Rock sphere 1	0.002683	0.002686	0.002683
Gangue-Rock sphere 2	0.002683	0.002686	0.002683

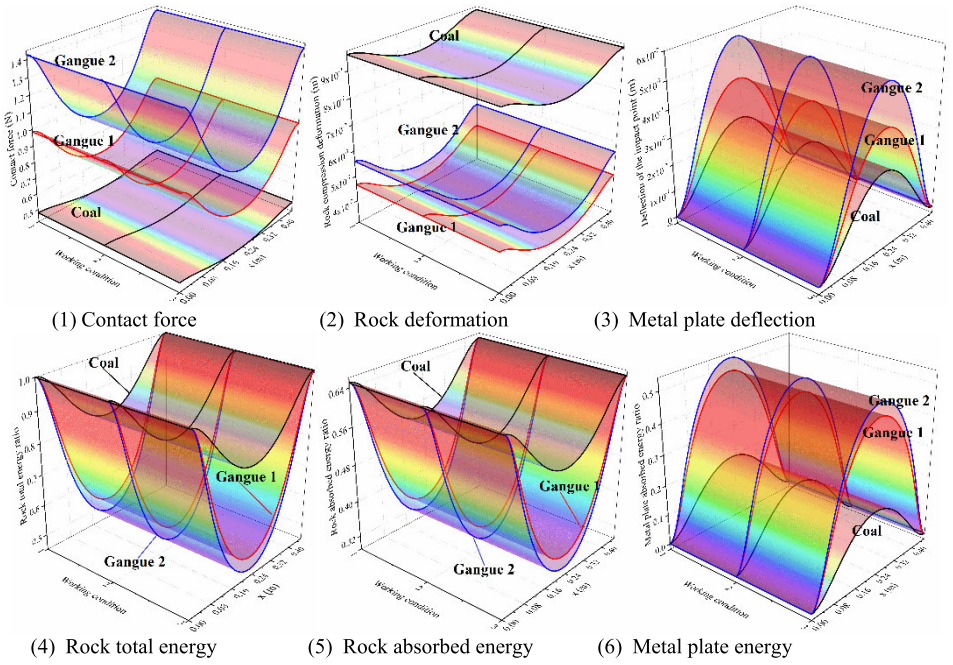

FIGURE 17. The system contact response when the supporting states changes.

TABLE 6. Bilateral fixed support.

Impact body	Contact force	Rock deformation (10^{-7}m)	Metal plate deflection (10^{-7}m)	Rock total energy ratio	Metal plate energy ratio
Coal-Rock sphere	0.42065148	8.77725888	2.61700466	0.80498950	0.19501103
Gangue-Rock sphere 1	0.66265566	3.57195473	4.12258853	0.51606256	0.48393805
Gangue-Rock sphere 2	0.91089265	4.15261761	5.66694865	0.47420472	0.52579516

that of the coal. The minimum yield velocity when three particles impacting the metal plate is 0.002683m/s. Take the impact velocity is 0.0025m/s, the compression deformation, the contact force, the impacted point's deflection curves of the metal plate and the energy conversion ratio curves are obtained and shown in Figure 17 (1)-(6) when above three particles impacts on the any axial position of the metal plate under different supporting states.

From the figures, for the three different supporting conditions, when impact on the same position of the metal plate with the same velocity, the maximum compression deformation of the gangue-rock with the same mass or the same size is far less than that of coal, while the maximum contact force and the deflection of the impacted point is far larger than that of coal. The ratio of the total energy absorbed and consumed by the coal-rock sphere and the ratio of the energy absorbed by the coal-rock sphere when reach the compression limit are all large than that of gangue with the same mass or the same size, while the ratio of the energy absorbed by the bending deformation of the metal plate when coal-tock sphere impact is less than that of gangue. The maximum contact force, the maximum compression deformation, the maximum deflection of the metal plate impact point, the ratio of the rock absorbed and consumed total energy, and the ratio of the energy absorbed by the metal plate when the three types of coal gangue impacting the midpoint of the three different supporting forms metal plate are shown in Tables 6-8.

By subtracting contact responses between the coal and the two type gangue in Tables 6-8, the differences between the contact response of the coal impact and the same mass or same volume gangue impact are obtained, as shown in Tables 9-10.

From Tables 6-10, when the metal plate axial midpoint is impacted, the differences of the maximum contact force

TABLE 7. Bilateral elastic support.

Impact body	Contact force	Rock deformation (10^{-7}m)	Metal plate deflection (10^{-7}m)	Rock total energy ratio	Metal plate energy ratio
Coal-Rock sphere	0.42061427	8.77674131	2.61677319	0.80487084	0.19497653
Gangue-Rock sphere 1	0.66251790	3.57145965	4.12173146	0.51588376	0.48373685
Gangue-Rock sphere 2	0.91068846	4.15199701	5.66567832	0.47402757	0.52555945

TABLE 8. Unilateral elastic unilateral fixed support.

Impact body	Contact force	Rock deformation (10^{-7}m)	Metal plate deflection (10^{-7}m)	Rock total energy ratio	Metal plate energy ratio
Coal-Rock sphere	0.42063287	8.77700008	2.61753126	0.80493016	0.19499379
Gangue-Rock sphere 1	0.66258677	3.57170715	4.12317175	0.51597315	0.48383747
Gangue-Rock sphere 2	0.91079054	4.15230726	5.66770423	0.47411613	0.52567732

TABLE 9. Contact response differences between the Coal-Rock sphere and the Gangue-Rock sphere 1.

Impact body	Contact force	Rock deformation (10^{-7}m)	Metal plate deflection (10^{-7}m)	Rock total energy ratio	Metal plate energy ratio
Bilateral fixed	-0.24200418	5.20530415	-1.50558387	0.28892694	-0.28892702
Bilateral elastic	-0.24190363	5.20528166	-1.50495827	0.28898708	-0.28876032
Unilateral elastic	-0.2419539	5.20529293	-1.50564049	0.28895701	-0.28884368

TABLE 10. Contact response differences between the Coal-Rock sphere and the Gangue-Rock sphere 2.

Impact body	Contact force	Rock deformation (10^{-7}m)	Metal plate deflection (10^{-7}m)	Rock total energy ratio	Metal plate energy ratio
Bilateral fixed	-0.49024117	4.62464127	-3.04994399	0.33078478	-0.33078413
Bilateral elastic	-0.49007419	4.6247443	-3.04890513	0.33084327	-0.33058292
Unilateral elastic	-0.49015767	4.62469282	-3.05017297	0.33081403	-0.33068353

and the energy ratio absorbed by the metal plate between the coal and the same mass or the same volume (same size) gangue under the bilateral fixed support are the largest, the differences of the above two responses under the unilateral elastic unilateral fixed support take the second place, and the differences of the above two responses under the bilateral elastic support are the least. The differences of the maximum total energy ratio absorbed by the rock between the coal and the same mass or the same volume (same size) gangue under the bilateral elastic support is the largest, the differences of the above response under the unilateral elastic unilateral fixed support take the second place, and the differences of the above response under the bilateral fixed support is the smallest. When the mass of the coal gangue are in the same, the differences of the maximum compression deformation between the coal and the same mass gangue under the bilateral fixed support are the largest, the differences of the above response under the unilateral elastic unilateral fixed support take the second place, and the differences of the above response under the bilateral elastic support are the least. When the size of the coal gangue are in the same, the differences of the maximum compression deformation between the coal and the same mass gangue under the bilateral elastic support are the largest, the differences of the above response under the unilateral elastic unilateral fixed support take the second place, and the differences of the above response under the bilateral fixed support are the least. Therefore, the elastic support and the increase of the elastic support end will reduce the difference of the maximum contact force and the energy ratio absorbed by the metal plate when coal gangue impact, increase the difference of the total energy absorbed and consumed by the rock, reduce the difference of the rock maximum compression deformation when same mass coal gangue impact, and increase the difference of the rock maximum compression deformation when same volume coal gangue impact. The impact point maximum deflection difference of the metal plate when coal gangue impact under the unilateral elastic and unilateral fixed support is the largest, while the difference of the above response under the bilateral elastic support is the smallest. Due to the impact point deflection of the metal plate under the unilateral elastic and unilateral fixed support is composed by the deflection of the simply supported beam and the deflection of the cantilever beam, and the together compression of the both ends springs will absorb the system energy. Thus, with the increase of the elastic support ends, the impact point deflection difference of the metal plate does not change monotonously during the coal gangue impact.

Figures 18-19 are the spring forces and the energy ratio absorbed by the spring in the bilateral elastic support and the unilateral elastic unilateral fixed support conditions. With the change of the impact position, the variation trend of the

TABLE 11. Spring response.

Impact body	Bilateral elastic support			Unilateral elastic unilateral elastic	
	Left force	Right force	Spring energy ratio	Spring force	Spring energy ratio
Coal-Rock sphere	0.10515357	0.10515357	0.00015316	0.10514789	0.00007657
Gangue-Rock sphere 1	0.16562947	0.16562947	0.00038000	0.16563043	0.00019000
Gangue-Rock sphere 2	0.22767212	0.22767212	0.00041285	0.22767528	0.00020643

TABLE 12. Spring response differences between the Coal-Rock sphere and the Gangue-Rock sphere.

Working condition	Bilateral elastic support		Unilateral elastic unilateral elastic	
	Left spring force	Spring energy ratio	Spring force	Spring energy ratio
Coal-Rock sphere minus Gangue-Rock sphere 1	-0.0604759	-0.00022684	-0.06048254	-0.00011343
Coal-Rock sphere minus Gangue-Rock sphere 2	-0.12251855	-0.00025969	-0.12252739	-0.00012986

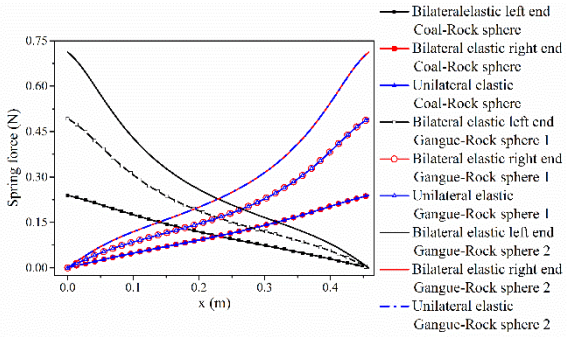

FIGURE 18. Spring force.

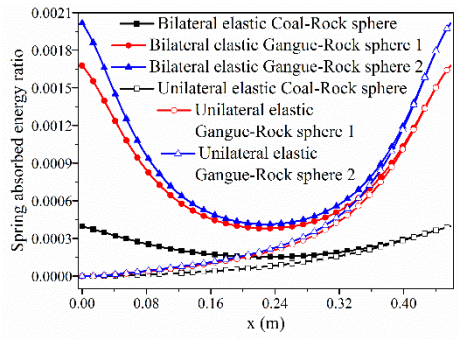

FIGURE 19. Spring energy.

spring force and the energy ratio absorbed by the spring when coal gangue impacting the metal plate is the same. When impacting the same position of the metal plate at the same velocity, the spring force generated by the coal impact under the bilateral elastic support and the unilateral elastic unilateral fixed support is less than that of the same mass or same volume gangue. The ratio of the energy absorbed by the spring when the gangue with the same mass or the same volume impact on the same point of the metal plate is larger than that of the coal under the bilateral elastic support and the unilateral elastic unilateral fixed support. When the three type of coal gangue impact the two different support form metal plate midpoint, the maximum spring force and the ratio of the energy absorbed by the spring are obtained as the Table 11, the response differences of the springs when the same mass or size coal gangue respectively impact the metal plates are shown in Table 12.

When the same mass or size coal gangue impacting the metal plate separately, the response difference of the left end single spring force under the bilateral elastic support is smaller than that of the unilateral elastic unilateral fixed support, but the energy ratio absorbed by springs is larger than that of the unilateral elastic unilateral fixed support. These indicate that the increase of the elastic support ends will increase the difference in the spring force under impact of coal gangue and decrease the difference in the energy ratio absorbed by the spring.

In the paper, the spring (i.e. the elastic support) is used to replace the prop and the tail beam jack, then we can speculate that the resulting response of the prop or the tail beam jack when coal gangue impacting the same position of the hydraulic powered support will also be different. Comprehensive analysis shows that coal-gangue identification is feasible according to the response differences such as the contact force, the metal plate deflection value and the changes of the hydraulic oil when coal gangue impact on the hydraulic powered support in top coal caving.

V. CONCLUSION

For further analysis of the collision contact behavior between coal gangue and the hydraulic support in top coal caving process, this paper simplified the impact collision behavior between the coal gangue particle and the different part of the hydraulic support to the coal gangue sphere vertical impact the bilateral fixed support, bilateral elastic support and the unilateral elastic unilateral fixed support metal plate system. Considering the energy absorbed and consumed by the sphere in the impact compression process, the energy absorbed by the deflection of the metal plate and the energy absorbed by the deformation of the metal plate, and with the aid of

the Flores contact theory, the simply supported beam and the cantilever beam bending deformation theory, the constant stiffness spring compression deformation theory and the energy conservation law, this paper establish system impact-contact dynamic model when the spherical rock impact the any axial position of the bilateral fixed support, the bilateral elastic support and the unilateral elastic unilateral fixed support metal plate. On the basis of the Drucker Prager criterion, we obtained the rock yield velocity model when the different support form metal plate is impacted. The influence of the elastic support, the impact position, the spring stiffness, and the metal plate length on the critical yield velocity and the system contact responses were studied. And the differences in the response when coal gangue impact were also analyzed. The following conclusions were obtained:

(1) When $k_{TD} = K_{Coal} = 5.11545 \times 10^8 N/m^{1.5}$, when the impact position changes from the left end of the metal plate to the right end, yield velocities of the Coal-Rock sphere and the Gangue-Rock sphere 1 all appears the approximate parabola form which increases first and then decreases. The rock minimum yield velocity appears at the left end of the plate (or appears at the both ends together), while the position where the maximum yield velocity appears close to the axial midpoint of the metal plate. The contact force, the rock compression deformation, the ratio of the rock total energy, and the ratio of the rock absorbed energy all appear the trend which decreases first and then increases. The minimum value of the above responses is close to the axial midpoint of the metal plate. The impact point deflection of the metal plate and the ratio of the energy absorbed by the bending deformation of the metal plate both appear the trend which increases first and then decreases. The left end spring force when impact the bilateral elastic support metal plate presents the decreases trend, the ratio of the energy absorbed by the spring decreases first and then increases, while its right end spring force and the spring force when impact the unilateral elastic unilateral fixed support metal plate both present the increase trend. The energy absorbed by the spring under the unilateral elastic unilateral fixed support presents the increases trend.

(2) The elastic support at the end of the metal plate and the number of the elastic support end when the spherical rock impact the metal plate will increase the rock initial yield velocity. When the same coal-rock sphere impact the bilateral elastic support metal plate and the unilateral elastic unilateral fixed support metal plate, the ratio of the energy absorbed by the spring under the bilateral elastic support is larger than that of the unilateral elastic unilateral fixed support. The exist of the elastic support will reduce the contact response such as the contact force, rock compression deformation, the metal plate impact point deflection, the rock total energy ratio, the rock absorbed energy ratio and the metal plate absorbed energy ratio.

(3) The changes of the spring stiffness will result in the shape changes of the rock yield velocity-impact position curve and the contact responses-impact position curves when impact the different position of the metal plate. With the increase of the spring stiffness, the rock yield velocity decreases when the same spherical rock impact the same position of the metal plate at the same velocity. The maximum contact force, the maximum compression deformation of the rock, the maximum spring force, the maximum ratio of the total energy absorbed and consumed by the rock, and the maximum ratio of the energy absorbed by the rock under the bilateral elastic support and the unilateral elastic unilateral fixed support all increase, while the maximum ratio of the energy absorbed by the spring decline. The impact point maximum deflection of the metal plate and the ratio of the energy absorbed by the metal plate under the bilateral elastic support gradually increase with the increase of the spring stiffness. The impact point deflection of the metal plate under the unilateral elastic unilateral fixed support decreases gradually, the ratio of the total energy absorbed by the metal plate decreases first and then increases with the increase of the spring stiffness.

(4) When the same spherical rock impact the same position of the metal plate at the same velocity, with the increase of the metal plate length, the rock yield velocity decreases. the system maximum contact force, the maximum compression deformation of the spherical rock, the ratio of the total energy absorbed and consumed by the rock as well as the ratio of the energy absorbed by the rock gradually decrease, while the impact point maximum deflection of the metal plate and the ratio of the energy absorbed by the metal plate increase gradually. The spring force at the left end of bilateral elastic support state increases gradually, while the spring force at its right end decreases gradually, the ratio of the total energy absorbed by the spring increases first and then decreases. The spring force and the energy ratio absorbed by the spring in the state of unilateral elastic unilateral fixed support both decrease gradually.

(5) When impact the same position of the metal plate at the same velocity, the maximum compression deformation, the ratio of the total energy absorbed and consumed by the same mass or volume (size) gangue-rock sphere and the ratio of the energy absorbed by the gangue -rock sphere all are far less than that of the coal, while the maximum contact force, the deflection of the impacted point, the ratio of the energy absorbed by the metal plate, the spring force and the ratio of the energy absorbed by the spring is larger than that of the coal. The elastic support and the increase of the elastic support end will reduce the difference of the maximum contact force and the energy ratio absorbed by the metal plate when the same mass or the same volume coal gangue impact, increase the difference of the total energy absorbed and consumed by the rock, reduce the difference of the rock maximum compression deformation when same mass coal gangue impact, and increase the difference of the rock maximum compression deformation when same volume coal gangue impact. And the increase of the elastic support ends will increase the difference in the spring force during the coal gangue impact and decrease the difference in the energy ratio absorbed by the spring.

The conclusions in this paper will supply theoretical references for calculating the initial yield velocity of rock under different impact conditions, and provide theory model for the contact response when the any axial position of the thin plate is vertically impacted. In addition, this paper will support a theoretical basis for studying the contact problem of the rock impact on the fixed support metal plate, the elastic support metal plate and the rigid-flexible combination support metal plate, and lay a theoretical foundation for further study on the contact-impact behavior between coal gangue granule and the hydraulic support in the top coal caving process. In the future work, in consideration of the deflection towards the width B of the metal plate, the finite element theory can be introduced into the construction and solution for the dynamic model where the metal plate is impacted by the rock sphere. By dividing the metal plate into the small size meshes, the macroscopic deformation and microscopic deformation of the metal plate would be considered comprehensively when the metal plate is impacted by particles, so as to achieve the more accurate calculation of the contact responses.

REFERENCES

[1] A. Vakilin and B. K. Hebblewhite, "A new cavability assessment criterion for longwall top coal caving," *Int. J. Rock Mech. Mining Sci.*, vol. 47, pp. 1317–1329, Dec. 2010. doi: 10.1016/j.ijrmms.2010.08.010.

[2] D. Khanal, D. Adhikary, and R. Balusu, "Evaluation of mine scale longwall top coal caving parameters using continuum analysis," *Mining Sci. Technol.*, vol. 21, pp. 787–796, Nov. 2011. doi: 10.1016/j.mstc.2011.06.027.

[3] I. G. Ediz, D. W. Dixon-Hardy, H. Akcakoca, and H. Aykul, "Application of retreating and caving longwall (top coal caving) method for coal production at GLE Turkey," *Mining Technol.*, vol. 115, no. 2, pp. 41–48, 2013. doi: 10.1179/174328606X103586.

[4] N. Wen, C. Weimin, Z. Lei, Z. Shuping, W. Hao, and Z. Liang, "Optimization research of hydraulic support in fully mechanized caving face," *Procedia Eng.*, vol. 84, pp. 770–778, 2014. doi: 10.1016/j.proeng.2014.10.495.

[5] Z. F. Dong, Y. J. Tang, J. H. Liu, H. X. Wu, Y. Q. Zhou, and J. Wu, "Mechanisms and virtual design of a new type of top-coal caving hydraulic support," in *Proc. 11th World Congr. Mechanism Mach. Sci.* Tianjin, China: China Machine Press, 2004, p. 5. doi: 10.3901/CJME.2004.supp.205.

[6] L. Yu, S.-H. Yan, H.-Y. Yu, and Z. Zhang, "Studying of dynamic bear characteristics and adaptability of support in top coal caving with great mining height," *Proc. Eng.*, vol. 26, pp. 640–646, 2011. doi: 10.1016/j.proeng.2011.11.2217.

[7] H. Minamoto and S. Kawamura, "Moderately high speed impact of two identical spheres," *Int. J. Impact Eng.*, vol. 38, pp. 123–129, Feb./Mar. 2011. doi: 10.1016/j.ijimpeng.2010.09.005.

[8] L. Vu-Quoc, X. Zhang, and L. Lesburg, "Normal and tangential force–displacement relations for frictional elasto-plastic contact of spheres," *Int. J. Solids Struct.*, vol. 38, pp. 6455–6489, Sep. 2001. doi: 10.1016/S0020-7683(01)00065-8.

[9] M. R. Brake, "The effect of the contact model on the impact-vibration response of continuous and discrete systems," *J. Sound Vibrat.*, vol. 332, pp. 3849–3878, Jul. 2013. doi: 10.1016/j.jsv.2013.02.003.

[10] Y. Du and S. Wang, "Energy dissipation in normal elastoplastic impact between two spheres," *J. Appl. Mech.*, vol. 76, no. 6, 2009, Art. no. 061010. doi: 10.1115/1.3130801.

[11] T. Krijt, C. Güttler, D. Heißelmann, C. Dominik, and A. G. G. M. Tielens, "Energy dissipation in head-on collisions of spheres," *J. Phys. D, Appl. Phys.*, vol. 46, Oct. 2013, Art. no. 435303. doi: 10.1088/0022-3727/46/43/435303.

[12] L. Vu-Quoc, X. Zhang, and L. Lesburg, "A normal force-displacement model for contacting spheres accounting for plastic deformation: Force-driven formulation," *J. Appl. Mech.*, vol. 67, no. 2, pp. 363–371, 2000. doi: 10.1115/1.1305334.

[13] X. Zhang and L. Vu-Quoc, "Modeling the dependence of the coefficient of restitution on the impact velocity in elasto-plastic collisions," *Int. J. Impact Eng.*, vol. 27, no. 3, pp. 317–341, 2002. doi: 10.1016/s0734-743x(01)00052-5.

[14] Y. Zhang and I. Sharf, "Validation of nonlinear viscoelastic contact force models for low speed impact," *J. Appl. Mech.*, vol. 76, no. 5, 2009, Art. no. 051002. doi: 10.1115/1.3112739.

[15] X. Zhang and L. Vu-Quoc, "An accurate elasto-plastic frictional tangential force-displacement model for granular-flow simulations: Displacement-driven formulation," *J. Comput. Phys.*, vol. 225, pp. 730–752, Jul. 2007. doi: 10.1016/j.jcp.2006.12.028.

[16] M. R. W. Brake, "An analytical elastic plastic contact model with strain hardening and frictional effects for normal and oblique impacts," *Int. J. Solids Struct.*, vol. 62, pp. 104–123, Jun. 2015. doi: 10.1016/j.ijsolstr.2015.02.018.

[17] J. Xie, M. Dong, S. Li, Y. Shang, and Z. Fu, "Dynamic characteristics for the normal impact process of micro-particles with a flat surface," *Aerosol Sci. Technol.*, vol. 52, no. 2, pp. 222–233, 2017. doi: 10.1080/02786826.2017.1396440.

[18] H. Xiao, M. J. Brennan, and Y. Shao, "On the undamped free vibration of a mass interacting with a Hertzian contact stiffness," *Mech. Res. Commun.*, vol. 38, pp. 560–564, Dec. 2011. doi: 10.1016/j.mechrescom.2011.07.012.

[19] R. Jackson, I. Chusoipin, and I. Green, "A finite element study of the residual stress and deformation in hemispherical contacts," *J. Tribol.*, vol. 127, no. 3, pp. 484–493, 2005. doi: 10.1115/1.1843166.

[20] O. Cermik, H. Ghaednia, and D. B. Marghitu, "Analytical study of the oblique impact of an elastic sphere with a rigid flat," in *Acoustics and Vibration of Mechanical Structures—AVMS*. Cham, Switzerland: Springer, 2018, pp. 33–40. doi: 10.1007/978-3-319-69823-6_4.

[21] R. L. Jackson and I. Green, "A finite element study of elasto-plastic hemispherical contact against a rigid flat," *J. Tribol.*, vol. 127, no. 2, pp. 343–354, 2005. doi: 10.1115/1.1866166.

[22] Y. A. Rossikhin, M. V. Shitikova, and M. S. Khalid, "Impact-induced internal resonance phenomena in nonlinear doubly curved shallow shells with rectangular base," in *Analysis and Modelling of Advanced Structures and Smart Systems*, vol. 81. Singapore: Springer, 2018, pp. 149–189. doi: 10.1007/978-981-10-6895-9_8.

[23] Y. W. Zhao, D. M. Maietta, and L. Chang, "An asperity microcontact model incorporating the transition from elastic deformation to fully plastic flow," *J. Tribol.*, vol. 122, no. 1, pp. 86–93, Jan. 2000. doi: 10.1115/1.555332.

[24] E. Willert, I. A. Lyashenko, and V. L. Popov, "Influence of the Tabor parameter on the adhesive normal impact of spheres in Maugis–Dugdale approximation," *Comput. Part. Mech.*, vol. 5, pp. 313–318, Jul. 2018. doi: 10.1007/s40571-017-0170-7.

[25] J. Jamari and D. J. Schipper, "Experimental investigation of fully plastic contact of a sphere against a hard flat," *J. Tribol.*, vol. 128, no. 2, pp. 230–235, 2006. doi: 10.1115/1.2164470.

[26] W. J. Stronge and A. D. C. Ashcroft, "Oblique impact of inflated balls at large deflections," *Int. J. Impact Eng.*, vol. 34, pp. 1003–1019, Jun. 2007. doi: 10.1016/j.ijimpeng.2006.04.006.

[27] E. Olsson and P.-L. Larsson, "On the tangential contact behavior at elastic–plastic spherical contact problems," *Wear*, vol. 319, pp. 110–117, Nov. 2014. doi: 10.1016/j.wear.2014.07.016.

[28] Z. Wang, H. Yu, and Q. Wang, "Layer-substrate system with an imperfectly bonded interface: Spring-like condition," *Int. J. Mech. Sci*, vol. 134, pp. 315–335, Dec. 2017. doi: 10.1016/j.ijmecsci.2017.10.028.

[29] R. Goltsberg and I. Etsion, "Contact area and maximum equivalent stress in elastic spherical contact with thin hard coating," *Tribol. Int.*, vol. 93, pp. 289–296, Jan. 2016. doi: 10.1016/j.triboint.2015.09.034.

[30] A. Ovcharenko, G. Halperin, G. Verberne, and I. Etsion, "*In situ* investigation of the contact area in elastic–plastic spherical contact during loading–unloading," *Tribol. Lett.* vol. 25, no. 2, pp. 153–160, 2007. doi: 10.1007/s11249-006-9164-y.

[31] M. R. Brake, "An analytical elastic-perfectly plastic contact model," *Int. J. Solids Struct.*, vol. 49, no. 22, pp. 3129–3141, Nov. 2012. doi: 10.1016/j.ijsolstr.2012.06.013.

[32] H. Minamoto and S. Kawamura, "Effects of material strain rate sensitivity in low speed impact between two identical spheres," *Int. J. Impact Eng.*, vol. 36, pp. 680–686, May 2009. doi: 10.1016/j.ijimpeng.2008.10.001.

[33] J. Jamari and D. J. Schipper, "An elastic–plastic contact model of ellipsoid bodies," *Tribol. Lett.*, vol. 21, no. 3, pp. 262–271, 2006. doi: 10.1007/s11249-006-9038-3.

[34] L. Vu-Quoc, L. Lesburg, and X. Zhang, "An accurate tangential force–displacement model for granular-flow simulations: Contacting spheres with plastic deformation, force-driven formulation," *J. Comput. Phys.*, vol. 196, pp. 298–326, May 2004. doi: 10.1016/j.jcp.2003.10.025.
[35] R. L. Jackson, R. Green, and D. B. Marghitu, "Predicting the coefficient of restitution of impacting elastic-perfectly plastic spheres," *Nonlinear Dyn.*, vol. 60, no. 3, pp. 217–229, 2010. doi: 10.1007/s11071-009-9591-z.
[36] L. Vu-Quoc and X. Zhang, "An elastoplastic contact force-displacement model in the normal direction: Displacement-driven version," *Proc. Roy. Soc. A, Math. Phys. Eng. Sci.*, vol. 455, pp. 4013–4044, Nov. 1999. doi: 10.1098/rspa.1999.0488.
[37] T. Wang, L. Wang, L. Gu, and D. Zheng, "Stress analysis of elastic coated solids in point contact," *Tribol. Int*, vol. 86, pp. 52–61, Jun. 2015. doi: 10.1016/j.triboint.2015.01.013.
[38] C. Thornton, S. J. Cummins, and P. W. Cleary, "On elastic-plastic normal contact force models, with and without adhesion," *Powder Technol.*, vol. 315, pp. 339–346, Jun. 2017. doi: 10.1016/j.powtec.2017.04.008.
[39] P. Peng, C. Di, L. Qian, and G. Chen, "Parameter identification and experimental investigation of sphere-plane contact impact dynamics," *Exp. Tech.*, vol. 41, pp. 547–555, Oct. 2017. doi: 10.1007/s40799-017-0195-0.
[40] Y. Yang, Q. Zeng, and L. Wan, "Contact response analysis of vertical impact between elastic sphere and elastic half space," *Shock Vib.*, vol. 2018, Nov. 2018, Art. no. 1802174. doi: 10.1155/2018/1802174.
[41] P. H. Bischoff, S. H. Perry, and J. Eibl, "Contact force calculations with a simple spring-mass model for hard impact: A case study using polystyrene aggregate concrete," *J. Impact Eng.*, vol. 9, no. 3, pp. 317–325, 1990. doi: 10.1016/0734-743X(90)90005-G.
[42] E. Rigaud and J. Perret-Liaudet, "Experiments and numerical results on non-linear vibrations of an impacting Hertzian contact. Part 1: Harmonic excitation," *J. Sound Vib.*, vol. 265, pp. 289–307, Aug. 2003. doi: 10.1016/S0022-460X(02)01262-2.
[43] Y. Yang, Q. Zeng, and L. Wan, "Dynamic response analysis of the vertical elastic impact of the spherical rock on the metal plate," *Int. J. Solids Struct.*, vol. 158, pp. 287–302, Feb. 2019. doi: 10.1016/j.ijsolstr.2018.09.017.
[44] K. L. Johnson, *Contact Mechanics*. Cambridge, U.K.: Cambridge Univ. Press, 1985.
[45] C. Braccesi and L. Landi, "A general elastic–plastic approach to impact analisys for stress state limit evaluation in ball screw bearings return system," *Int. J. Impact Eng.*, vol. 34, pp. 1272–1285, Jul. 2007. doi: 10.1016/j.ijimpeng.2006.06.005.
[46] H. Wang, X. Yin, X. Qi, Q. Deng, B. Yu, and Q. Hao, "Experimental and theoretical analysis of the elastic-plastic normal repeated impacts of a sphere on a beam," *Int. J. Solids Struct.*, vol. 109, pp. 131–142, Mar. 2017. doi: 10.1016/j.ijsolstr.2017.01.014.
[47] R. Boettcher, A. Russell, and P. Mueller, "Energy dissipation during impacts of spheres on plates: Investigation of developing elastic flexural waves," *Int. J. Solids Struct.*, vols. 106–107, pp. 229–239, Feb. 2017. doi: 10.1016/j.ijsolstr.2016.11.016.
[48] C. Thornton, Z. M. Ning, C.-Y. Wu, M. Nasrullah, and L.-Y. Li, "Contact mechanics and coefficients of restitution," in *Granular Gases* (Lecture Notes in Physics), vol. 564. Berlin, Germany: Springer, 2001, pp. 184–194. doi: 10.1007/3-540-44506-4_9.
[49] L. Kogut and I. Etsion, "Elastic-plastic contact analysis of a sphere and a rigid flat," *J. Appl. Mech.*, vol. 69, no. 5, pp. 657–662, 2002. doi: 10.1115/1.1490373.
[50] P. Flores, "A parametric study on the dynamic response of planar multibody systems with multiple clearance joints," *Nonlinear Dyn.*, vol. 61, pp. 633–653, Sep. 2010. doi: 10.1007/s11071-010-9676-8.
[51] P. Flores, M. Machado, M. T. Silva, and J. M. Martins, "On the continuous contact force models for soft materials in multibody dynamics," *Multibody Syst. Dyn.*, vol. 25, pp. 357–375, Mar. 2011. doi: 10.1007/s11044-010-9237-4.
[52] P. Flores, C. S. Koshy, H. M. Lankarani, J. Ambrósio, and J. C. P. Claro, "Numerical and experimental investigation on multibody systems with revolute clearance joints," *Nonlinear Dyn.*, vol. 65, pp. 383–398, Sep. 2011. doi: 10.1007/s11071-010-9899-8.
[53] P. Flores, J. Ambrósio, J. C. P. Claro, and H. M. Lankarani, "Dynamic behaviour of planar rigid multi-body systems including revolute joints with clearance," *Proc. Inst. Mech. Eng. K, J. Multibody Dyn.*, vol. 221, no. 2, pp. 161–174, 2007. doi: 10.1243/14644193JMBD96.
[54] J. Alves, N. Peixinho, M. T. da Silva, P. Flores, and H. M. Lankarani, "A comparative study of the viscoelastic constitutive models for frictionless contact interfaces in solids," *Mech. Mach. Theory*, vol. 85, pp. 172–188, Mar. 2015. doi: 10.1016/j.mechmachtheory.2014.11.020.
[55] K. Ye, L. Li, and H. Zhu, "A note on the Hertz contact model with nonlinear damping for pounding simulation," *Earthquake Eng. Struct. Dyn.*, vol. 38, pp. 1135–1142, Jul. 2009. doi: 10.1002/eqe.883.
[56] T. Yu, J. G. Teng, Y. L. Wong, and S. L. Dong, "Finite element modeling of confined concrete—I: Drucker–Prager type plasticity model," *Eng. Struct.*, vol. 32, pp. 665–679, Mar. 2010. doi: 10.1016/j.engstruct.2009.11.014.
[57] X. Ding and G. Zhang, "Coefficient of equivalent plastic strain based on the associated flow of the Drucker–Prager criterion," *Int. J. Non-Linear Mech.*, vol. 93, pp. 15–20, Jul. 2017. doi: 10.1016/j.ijnonlinmec.2017.04.018.
[58] R. Rahimi, "The effect of using different rock failure criteria in wellbore stability analysis," M.S. thesis, Missouri Univ. Sci. Technol., Graduate School, Rolla, MO, USA, 2014.
[59] G.-Y. Hou and X.-S. Niu, "Perfect elastoplastic solution of axisymmetric circular openings in rock mass based on Levy-Mises constitutive relation and D-P yield criterion," *Rock Soil Mech.*, vol. 30, no. 6, pp. 1555–1562, 2009. doi: 10.16285/j.rsm.2009.06.003.
[60] X. Y. Yun, "Geomechanical behaviour of biaxially loaded rock," Ph.D. dissertation, McGill Univ., Dept. Mater. Eng., Montreal, QC, Canada, 2008.
[61] L. R. Alejano and A. Bobet, "Drucker–prager criterion," *Rock Mech. Rock Eng.*, vol. 45, no. 6, pp. 995–999, 2012. doi: 10.1007/s00603-012-0278-2.
[62] V. Brizmer, Y. Kligerman, and I. Etsion, "The effect of contact conditions and material properties on the elasticity terminus of a spherical contact," *Int. J. Solids. Struct.*, vol. 43, pp. 5736–5749, Sep. 2006. doi: 10.1016/j.ijsolstr.2005.07.034.
[63] Q. Zeng, Y. Yang, X. Zhang, L. Wan, J. Zhou, and G. Yin, "Study on metal plate vibration response under Coal–Gangue impact based on 3D simulation," *Arabian J. Sci. Eng.*, vol. 44, pp. 7567–7580, Sep. 2019. doi: 10.1007/s13369-019-03853-3.

YANG YANG received the B.E. degree in machine design and automation from the Shandong University of Science and Technology, in 2015, where he is currently pursuing the Ph.D. degree. His research interests include contact mechanics, coal gangue interface recognition, signal processing, mechanical design electromechanical integration, and intelligent control.

QINGLIANG ZENG received the Ph.D. degree in machine design and theory from the China University of Mining and Technology, in 2000. He is currently a Professor with the Shandong University of Science and Technology and Shandong Normal University. He has participated more than 40 projects funded by the National Sci-Tech Support Plan, the National 863 Program, and the Natural Science Foundation of China. He has published more than 90 articles as the principle person. His research interests include electromechanical integration, condition monitoring and fault diagnosis, and virtual prototype.